Fundamental physics and applications of skyrmions: A review

Kang Wang [*], Vineetha Bheemarasetty, Junhang Duan, Shiyu Zhou, Gang Xiao [*]

Department of Physics, Brown University, Providence, RI 02912, USA

ABSTRACT

Beyond-CMOS computational paradigms are necessary to solving the problems that we face with modern computers in achieving scalability, low energy consumption, reduced latency, and enhanced complexity. Spintronic systems that exploit electron spin in conjunction with its charge are promising candidates given their demonstration of hardware implementations of low-energy-consumption and high-speed computing architectures. Magnetic skyrmions are tiny magnetic swirls that hold great potential in innovative electronic devices owing to their desirable properties of long-term stability, small size, and highly efficient controllability by various external stimuli. In this topic review, we address the fundamental physics of the static, global and local dynamic properties of skyrmions and provide an overview of recent advances in computational models that utilize these unique properties. A discussion on the challenges lying ahead is also provided.

1. Introduction

Since the invention of the transistor in the mid-20th century, CMOS technologies have progressed significantly to read, write, and store vast amounts of data. Despite their prevalence and success in attaining high gain and signal-to-noise ratios, current semiconductor technologies face challenges in achieving scalability, low energy consumption, and reduced latency [1,2]. Most modern-day computers are based on the von Neumann computing architecture which is characterized by a single, shared memory for programs and data [3]. This restriction leads to a bottleneck that has become strained from the exponential increase in demand for data storage and processing in recent years. The physical separation between processing and memory units in the von Neumann architecture gives rise to a "memory wall" by which processing power and execution speed are significantly reduced. In-memory computing resolves this issue of separation but fails as a high-performance hardware-software integration architecture [4]. And although modified CPU designs that enhance performance through parallelization have advantages to in-memory computing, they do not address the fundamental limitations of current CMOS computers [5]. On the other hand, von Neumann computers also meet challenges in efficiently addressing issues of optimization, invertible logic, and recognition. These constraints have led to a significant drive for the implementation of post-von Neumann computing architectures as alternatives to CMOS-based technologies.

Recent efforts in the field of solid-state condensed matter physics have been centered on a new class of devices referred to as *spintronics*. The advantage that spintronic devices have over their charge-based CMOS counterparts is that they utilize electron spin in conjunction with its charge [6–8]. This provides an additional degree of freedom to manipulate the magnetic moment associated with the spin and reduces energy consumption while inducing significant, measurable changes in the magnetic system. These types of devices are attractive in the development of post-von Neumann architectures because they are characterized by a high degree of scalability, immunity to the resistance drift and phase relaxation of electrons, high retention time, non-volatile memory, high endurance, high working speed, and low power consumption [8–11].

Recent advancements that have yielded promising spintronic device prototypes make use of the interplay between spin torques and topological spin textures [12–14]. The resulting magnetization dynamics can be further manipulated via applied fields and currents, leading to the development of spintronic devices. One of the key elements of spintronic technology is the magnetic tunneling junction (MTJ) which was first successfully fabricated in the mid-1990s [15–17]. This device architecture consists of two ferromagnetic layers separated by a thin insulating layer and can exhibit high tunneling magnetoresistance (TMR) [18–24]. The magnetization of the free layer may be manipulated by polarized current-induced spin-transfer torque (STT) which originates from the spin-filter effect of the reference layer [25–27] as well as from spin-orbit torque (SOT) from strong spin–orbit coupling (SOC) of the adjacent heavy metal layer [28–30]. High TMR and current-driven manipulation of the magnetization are critical for Magnetoresistive Random Access Memory (MRAM) [31–36] and magnetic field sensor applications [37–44] which have been commercialized in recent years. He et al. and Zhang et al. have shown that superior sensing capability may be

---

achieved by incorporating a superparamagnetic state [39] or a vortex magnetization state [38] in the free layer. The interplay between spin torques and these magnetization states yields a wide variety of unconventional computing applications that have also been theorized and are currently the center of many research efforts. Examples include superparamagnetic MTJs [45–49], spin-torque nano-oscillators [50–52], and current-driven domain-wall motion [53–57], for stochastic and neuromorphic computing applications.

Magnetic skyrmions are vortex-like noncollinear spin textures (Fig. 1 (a) and (b)) that can appear in a wide variety of magnetic systems [14,58,59]. These include non-centrosymmetric bulk magnets with either chiral, polar or D_{2d} symmetry [60–69], heterostructures with inversion symmetry broken at interfaces [70–77], and magnetically frustrated materials with achiral lattices and competing interactions [78–81]. Magnetic skyrmions have also been observed in some confined geometries such as nanowires and nanodots [82–85]. Magnetic skyrmions are tiny particle-like entities with sizes ranging from a few nanometers to several microns [66–69,73,74,77]. They are topologically protected with topological charges $Q = \int q(\mathbf{r}) dxdy = \pm 1$ where $q(\mathbf{r}) = \mathbf{m} \bullet (\partial_x \mathbf{m} \times \partial_y \mathbf{m})/4\pi$ is the topological charge density and $\mathbf{m}$ is the normalized magnetization. The topology of skyrmions allows them to have a high stability over time as they cannot be continuously changed into other trivial magnetic structures such as magnetic bubbles, magnetic domain walls, or a uniform magnetization state with a zero topological charge. Due to their non-trivial topological protection, skyrmions are extremely metastable in a field polarized environment and are non-dissipative. Many studies have illustrated that skyrmions may be reliably manipulated by small external fields [86–89] and currents [71–74,76] as well as temperature [90–93]. As a result, they promise low power operation at room temperature. Even with a small field and current, skyrmions exhibit high endurance and very high speeds that promote them as reliable information carriers. These desirable properties of skyrmions make them effective agents in next-generation beyond-CMOS data storage, logic, stochastic computing, and neuromorphic computing applications. Moreover, their mobility in space can more easily facilitate the integration of computing with data storage in a single die to achieve efficient communication that cannot be realized in traditional von Neumann architectures.

In view of these properties of skyrmions along with their CMOS compatibility, it is useful to discuss the fundamental physics of skyrmions and their applications in skyrmion-based electronic computational architectures. This review article is intended to build a broad view of skyrmion electronic applications and address the underlying physics.

2. Static, global, and local dynamic properties of skyrmions

Static properties of skyrmions. The existence of magnetic skyrmions is a direct consequence of the delicate interplay between competing energy terms. These include the anisotropy (U_{ani}) [94,95], exchange interaction (U_{ex}), antisymmetric Dzyaloshinskii-Moriya interaction (DMI) (U_{DMI}) [96–98], Zeeman (U_{Zeeman}), and demagnetization (U_{demag}) energies.

$$U = U_{ani} + U_{ex} + U_{DMI} + U_{Zeeman} + U_{demag}. \tag{1}$$

In this equation, $U_{ani} = \int d^2 x K_u (\mathbf{u} \bullet \mathbf{m})\mathbf{u}$ where K_u is the anisotropy constant and $\mathbf{u}$ is a unit vector indicating the anisotropy direction, $U_{ex} = \int d^2 x A(\nabla \mathbf{m})^2$ where A is the exchange stiffness, $U_{Zeeman} = -\mu_0 \int d^2 x M_S \mathbf{m} \bullet \mathbf{H}_{ext}$ where M_S is the saturation magnetization and $\mathbf{H}_{ext}$ is the external magnetic field, and $U_{demag} = -\frac{1}{2}\mu_0 \int d^2 x M_S \mathbf{m} \bullet \mathbf{H}_{demag}$ where $\mathbf{H}_{demag}$ is the demagnetization field. In non-centrosymmetric bulk magnets, $U_{DMI} = \int d^2 x D \mathbf{m} \bullet (\nabla \times \mathbf{m})$ which favors Bloch-type magnetic configuration (Fig. 1(a)), while in magnetic heterostructures with inversion symmetry broken at interfaces, $U_{DMI} = \int d^2 x D[m_z \text{div } \mathbf{m} - (\mathbf{m} \bullet \nabla)m_z]$ and favors Néel-type objects (Fig. 1(b)). Here, D is the bulk or interfacial DMI constant. These material parameters determine the skyrmion size and domain-wall width which are two fundamental quantities describing a magnetic skyrmion. In non-centrosymmetric bulk magnets where a helimagnetic structure is observed at zero-field while skyrmion lattices are observed in the nonzero, finite field range the periodicity is typically determined by A/D [99–102]. This, however, is not the case in magnetic heterostructures where isolated skyrmions are observed whose size is also sensitive to the anisotropy as well as the applied fields [73–75,103–107]. There have been numerous theoretical studies on the isolated skyrmion size [104,108,109]. Wang et al. has presented a general theory on the skyrmion size and domain-wall width [108]. The theoretical calculations are in good agreement with many simulations and experiments for a wide range of material parameters. The proposed theory suggests a mechanism to engineer material parameters to yield smaller skyrmions which are crucial to addressing the issue of spatial cost in device applications.

Although magnetic parameters are fixed once a system is fabricated, they may be further manipulated by various controls including the voltage [110–114] as well as chemisorption and desorption methods [115–117]. Wang et al. has reported an electric field-induced switching of individual skyrmions in a nanoscale magnetic heterostructure (Fig. 1
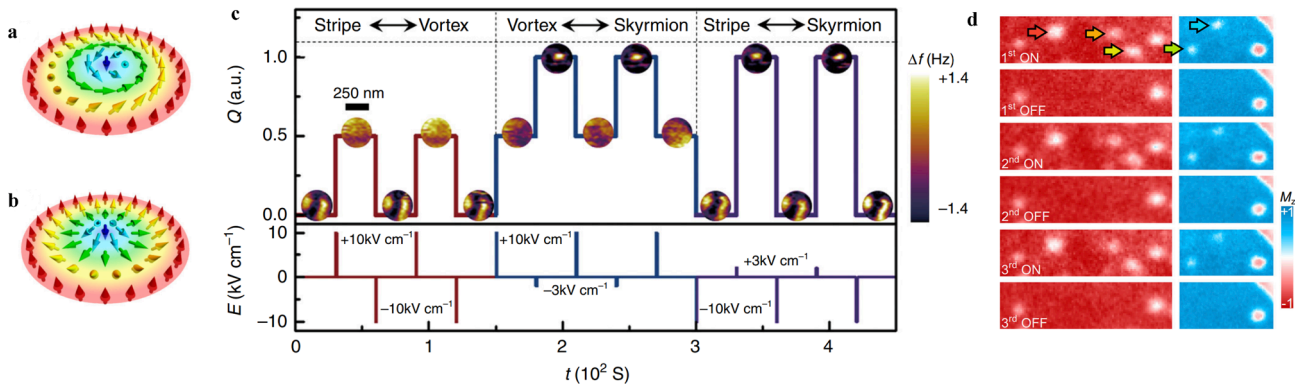
Fig. 1. a Bloch-type and **b** Néel-type skyrmion configurations [59]. **c** Switching of individual skyrmions in a nanodot with a diameter of 350 nm induced by a pulsed electric field E. The top panel shows fluctuations in the topological number Q over time in response to an applied 1 ms voltage pulse (bottom panel). The different magnetic domains included here are the skyrmion ($Q = 1$), vortex ($Q = 0.5$), and stripe ($Q = 0$). Switching between these domains is illustrated by magnetic force microscope (MFM) images and quantified by the energy required to make the transition [110]. **d** Experimental results of reversible writing/deleting of magnetic skyrmions in a Ni/Co/Pd/W(110) thin film via chemisorption and desorption of hydrogen gas. An ON cycle involves supplying a dose of hydrogen gas to write skyrmions. An OFF cycle allows sufficient time for spontaneous hydrogen desorption and recovery of the magnetization to the initial state. Red and blue regions refer to the evolution of the perpendicular magnetization of the sample [115].

(c)) [110]. An individual skyrmion can be converted into either a magnetic strip or a vortex state through the electric field-induced strain and the strain-mediated modification of the effective PMA and DMI. Chen et al. has shown that the effective PMA and DMI of magnetic heterostructures may also be altered via absorption or desorption of light elements such as hydrogen and oxygen [115–117]. This may lead to a modification of the spin chirality at magnetic domain walls and may promote the creation and deletion of skyrmions (Fig. 1(d)). This magneto-ionic functionality may be useful in constructing low-power-consumption, non-volatile memory devices and artificial synapses based on multistate skyrmions.

Typically, the magnetic parameters tend to be inhomogeneous or anisotropic in magnetic systems [118]. This may affect the detailed spin texture of a skyrmion [76,118–120]. For example, Cui et al. has reported

Néel-type elliptical skyrmions in a laterally-asymmetric magnetic multilayer where the anisotropic PMA and DMI may exist [119]. Jena et al. has also observed elliptical Bloch-type skyrmions in $Mn_{1.4}Pt_{0.9}Pd_{0.1}Sn$ with D_{2d} symmetry and an anisotropic DMI [121]. Wang et al. has verified that by interacting with local pinning centers induced by the inhomogeneity, a skyrmion may be either in a small-skyrmion or a large-skyrmion configuration [76]. Although multiple studies have explored the effects of pinning on skyrmions [99,122–130], little is known about the energy profiles induced by different kinds of pinning centers and how the static configurations of skyrmions are affected by the skyrmion interactions, pinning strengths, and thermal effects. It is essential to develop a methodology for visualizing the energy profiles of skyrmion pinning as they are crucial to the reliable positioning and guiding of skyrmions as well as to avoiding skyrmion
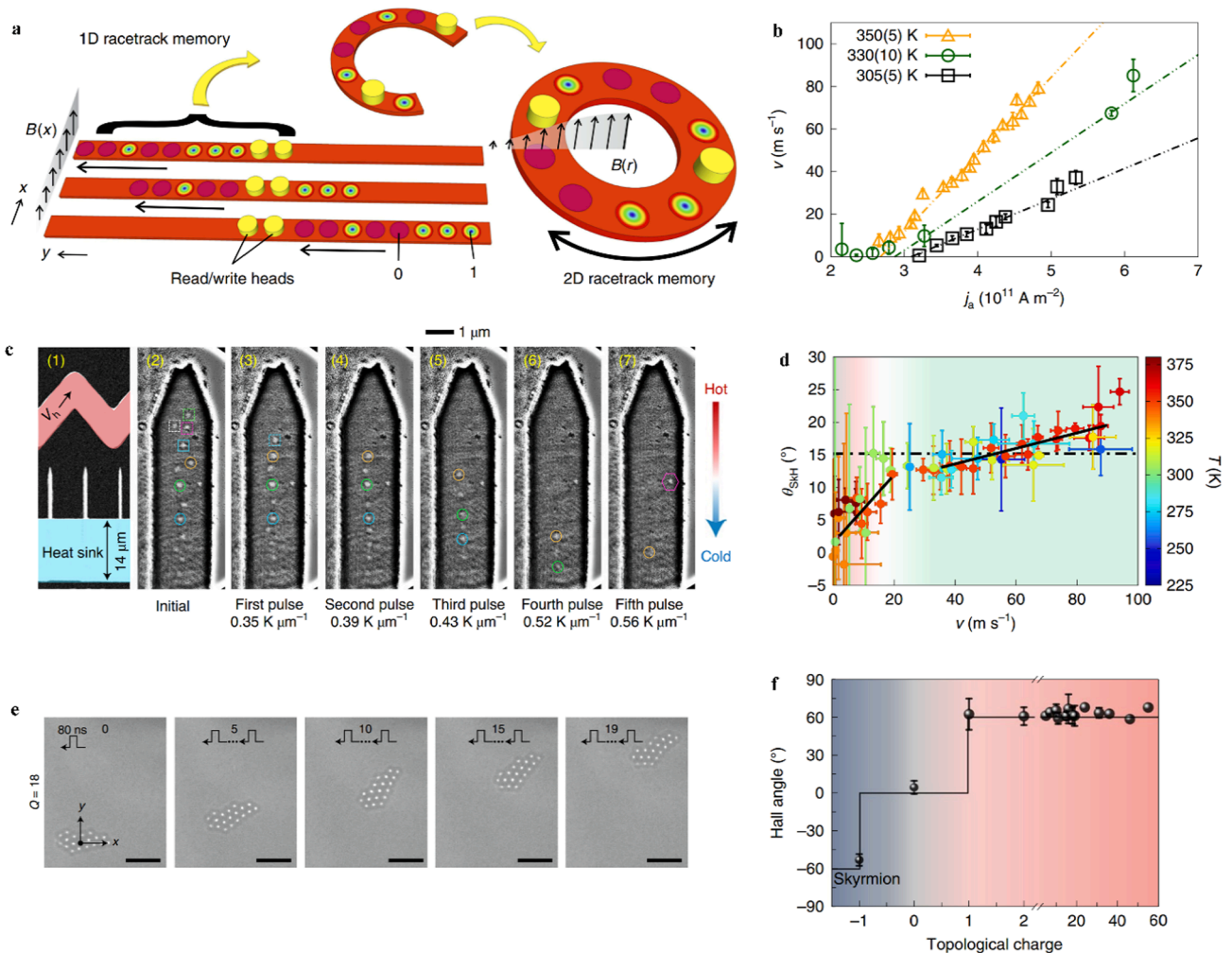
Fig. 2. a Schematic of a racetrack memory concept. In one-dimensional racetrack memory, the presence or absence of skyrmions is used to encode bits 1 or 0, respectively, as the skyrmion stream moves across the track past read/write heads. Further degrees of freedom can be accessed by bending these strips into circles to create two-dimensional racetrack memory. Motion of skyrmions in this disk can be achieved by an external applied field gradient $\mathbf{B}(r)$ [86]. **b** Plot of skyrmion velocity as a function of current density at several sample temperatures. Variation in the slopes stems from spin-orbit torque (SOT). The results are obtained in a [Pt (2.7 nm)/CoFeB(0.86 nm)/MgO(1.5 nm)]$_{15}$ multilayer stack [153]. **c** Illustration of thermally induced skyrmion motion. (1) Scanning electron microscopy (SEM) image of the device. 500 ms pulse voltages V_h are applied to the Ta/Pt heater. A temperature gradient is created across the [Ta/CoFeB/MgO]$_{15}$ nanowires between the heater and the heat sink via thermal dissipation in the insulating Si_3N_4 thin layer underneath. (2)-(7) Unidirectional diffusion of skyrmions observed from hot to cold regions in response to 500 ms pulse voltages V_h. Here, several different dynamics are observed including pinned skyrmions, skyrmion annihilation and long-range skyrmion diffusion [93]. **d** Skyrmion Hall angle (SHA) θ_{SKH} as a function of skyrmion velocity at various temperatures in the same structures as **b**. Two distinct regions are observed. The creep regime (red region) is characterized by a steep increase in the SHA with velocity while in the flow regime (green region) the slope is notably smaller. The theoretical disorder-free SHA for skyrmions is indicated by the black dashed line [153]. **e** Lorentz transmission electron microscopy (TEM) images of current-induced motion of skyrmion bundles with $Q = 18$. A series of 80 ns pulses are applied in the -x direction at a perpendicular field of 100 mT. As expected by the skyrmion Hall effect, the bundles move in the + x direction with a notable transverse motion in the y direction [164]. **f** Plot of SHA as a function of the topological charge Q of skyrmion bundles. It is evident that the sign of the Hall angle is dependent on the sign of the topological charge. Furthermore, the Hall angle is seemingly independent of the applied current density, external field, and Q [164].

annihilation. For more general reviews of the interaction of skyrmions with quenched disorder or pinning, we refer the reader to the Ref. [118].

Global dynamic properties of skyrmions. The spin dynamics are governed by the Landau-Lifshitz-Gilbert (LLG) equation,

$$\dot{\mathbf{m}} = -\frac{\gamma_L}{M_S} \mathbf{m} \times \left(-\frac{\delta U}{\delta \mathbf{m}} \right) + \alpha \mathbf{m} \times \dot{\mathbf{m}}, \tag{2}$$

where γ_L and α are the gyromagnetic ratio and Gilbert damping constant, respectively. The first and second terms on the right-hand side are field-like torque and damping-like torque, respectively. Skyrmions are electron spin ensembles with a topology that allows them to be reliably manipulated as particle-like entities.

Skyrmions can be created, manipulated, and deleted by various external stimuli such as applied magnetic fields [70,86–89], electrical currents [71–74,76], temperature [90–93], bias voltage [110–114], and chemisorption and desorption [115–117] methods. Zhang et al. has illustrated skyrmion motion under the influence of a magnetic field gradient (Fig. 2(a)) [86]. Migita et al. has verified AC magnetic field-driven skyrmion motion in an asymmetric angelfish-type racetrack [89]. Electrical currents are also effective in manipulating skyrmions. Spin currents can be generated by passing a charge current through a magnetic layer which then exerts a Zhang-Li STT on the spins [131]. This can be well described by a diffusive exchange-torque model. Equally as effective, spin currents can also be generated by the spin-filter effect [25–27] or by the SOC effect such as the Rashba [132] and spin Hall effects [133–142] which exert the Slonczewski STT [143,144]. The STT arising from the SOC effect is also known as the SOT. Zhang-Li STT may have a negligible effect on spin dynamics compared to the Slonczewski STT effect [75]. It has been shown that a single skyrmion can be created by passing a current through a constricted geometry [70,74,145,146], by the presence of local defects [70,147,148], or by applying a localized spin torque [103,149,150]. These cause the magnetization to flip first in a defined region forming a trivial magnetic bubble with $Q = 0$ followed by a transformation into a skyrmion stabilized by the DMI. Skyrmions may also be transformed from stripe domains with the application of a spin current [75,151,152]. Wang et al. has found that an applied current leads to the generation and/or deletion of topological defects through modifications of the domain wall motion and the magnetic configurations within the domain walls [75]. This may also lead to the transformation of a labyrinthine domain phase in the orientational order. Whether the labyrinthine domain phase transforms into a dense array of skyrmions or simply changes in its orientation order depends on the strengths of the applied current pulse and the external magnetic field. Skyrmions can move under the influence of currents [71,72,99,122,124,145,149,153] and a high propagation velocity (> 100m/s) may be achieved even under a low current density (Fig. 2(b)). Annihilation of a skyrmion is generally achieved by driving it to the boundary of a confined geometry [145,149], or by employing a localized spin torque to overcome the energy barrier between stable skyrmion and ferromagnetic states [103]. Skyrmion creation, motion, and deletion have also been observed in the presence of thermal gradients where magnonic spin torques may play a role (Fig. 2 (c)) [90,93], and under influences of a bias voltage [112,114]. Absorption and desorption of light elements has also been demonstrated to contribute to skyrmion creation and annihilation [115]. Manipulations of skyrmions by the bias voltage [110–114] and chemisorption and desorption [115–117] methods are consequential to manipulations of material parameters.

The center-of-mass motion of a magnetic texture can be approximately described by the Thiele equation.

$$G \times v + \alpha D v - F = 0, \tag{3}$$

which can be rigorously derived from the LLG equation [154,155]. In Eq. (3), the first and second terms are functions of the velocity $\mathbf{v}$ of the magnetic texture and are known as Magnus force and dissipative force,

respectively. The gyro coupling vector only has a z-component $G = 4\pi Q$. D is the dissipation tensor with $D_{ij} = \int \partial_i m \cdot \partial_j m dx dy$. $\mathbf{F}$ is the force either from the external stimuli or from spatial variations in material parameters ($\mathbf{F} = -\frac{\gamma_L}{M_S d} \nabla U$). In magnetic heterostructures with broken inversion symmetry, the force induced by the SOT can be written as $F = -\frac{1}{2}\gamma_L \beta T$ where $\frac{1}{2}\gamma_L \beta = \frac{\gamma_L \Theta_{SH} \hbar}{2M_S ed}$, the vector $T = \int d^2 x (e_z \times J_e) \cdot (\nabla m \times m)$, γ_L is the gyromagnetic ratio, Θ_{SH} is the spin Hall angle of the spin Hall solid, $\hbar$ is the reduced Planck constant, e is the elementary charge, d is the magnetic layer thickness, $\mathbf{e}_z$ is the unit vector along the z axis, and $\mathbf{J}_e$ is the charge current flowing through the spin Hall solid. For a rigid skyrmion, $T = \frac{\pi^2}{2} R \Gamma (e_z \times J_e)$ with the tensor $\overleftrightarrow{\Gamma} = \begin{bmatrix} 0 & -1 & 0 \\ 1 & 0 & 0 \\ 0 & 0 & 0 \end{bmatrix}$, and R is the skyrmion radius.

For magnetic skyrmions, the topological charge $Q = \pm 1$ and the Magnus force in Eq. (3) is non-zero, leading to an additional transverse component of motion accompanying the longitudinal motion of skyrmions along the driving force direction (Fig. 2(d)). The transverse motion direction reverses with reversing the polarity of skyrmions. This phenomenon is known as the skyrmion Hall effect [71,72] and is usually used to distinguish skyrmions from other trivial magnetic bubbles. It is known that trivial magnetic bubbles with $Q = 0$ do not experience the Magnus force and therefore the skyrmion Hall effect is imperceptible. The Thiele equation may also be applied to many other magnetic textures such as magnetic skyrmioniums [156–158] and antiferromagnetic skyrmions [158–163] with $Q = 0$, as well as skyrmion bundles with variable integer Q values (Fig. 2(e) and (f)) [164,165]. The experimental observation of multi-Q skyrmion bundles further expands the family of magnetic structures, which may prove useful in future spintronic devices. The skyrmion Hall angle (SHA) is a fundamental parameter characterizing the degree of deflection of the skyrmion motion relative to the driving force and is determined by the skyrmion polarity, configuration, and damping properties of the magnetic films [71,72,153]. Although the intrinsic SHA is independent of the driving force, the skyrmion motion may be influenced strongly by the driving force owing to the unavoidable pinning effects on skyrmions [71,72,99,122,124,149,153]. The skyrmion Hall effect is usually undesirable in skyrmion motion-based device applications, and many notable approaches to suppressing this effect have been recently recognized. These methods include modifying the interaction potential of skyrmions with geometry boundaries [145,166,167] and local defects [168] as well as implementing alternative magnetic textures such as skyrmioniums [156–158] and antiferromagnetic skyrmions [158–163].

Skyrmion motion was first proposed in racetrack memory devices in 2013 by Fert et al. [169] The concept of racetrack memory was first introduced in 2008 by Parkin et al. based on domain walls [170]. This aims to solve the constraints of modern-day CMOS devices which are approaching fundamental physical limits. In skyrmion racetrack memory, the digital information is encoded by the existence or absence of a single skyrmion (Fig. 2(a) and 3(a)) [145,167,171–173] or sequence of skyrmions and other magnetic textures such as bobbers (Fig. 3(b)) [174,175] and antiskyrmions [62]. Interactions of a skyrmion with adjacent spin textures, local defects, and geometrical edges may affect the feasibility of memory devices. In skyrmion racetrack memory, it is crucial to correct or revise skyrmion information in a controlled manner. Wang et al. has proposed and demonstrated through simulations an experimentally feasible method to modify a train of skyrmion information by a small electrical current [145]. Wang et al. has also studied a three-terminal racetrack memory in which an isolated skyrmion can be generated and annihilated by a gate voltage pulse (Fig. 3(a)). From this, one can modify a train of skyrmion codes in a controlled manner, which can then be detected at the collector. Despite the intriguing properties of skyrmion racetrack memory, its technological implementation may be limited by pinning effects, the stability of skyrmions over time and space, edge roughness, and the intrinsic skyrmion Hall effect which may
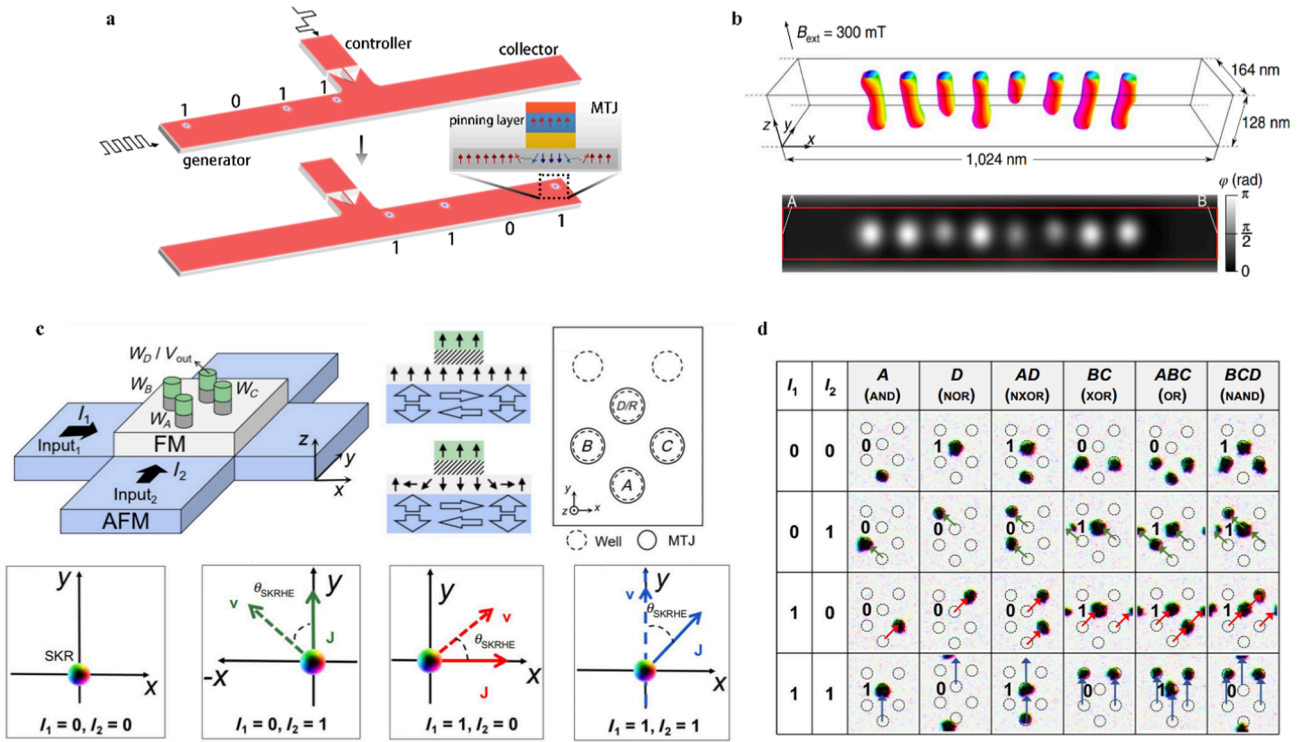
Fig. 3. a Schematic of a three-terminal racetrack memory device. The generator creates the skyrmion which is then detected at the collector. The presence or absence of a skyrmion is used to encode a bit 1 or 0, respectively. A voltage pulse can be applied in the controller terminal to create or delete a skyrmion, thereby enabling the modification of the skyrmion information in a controlled manner. This figure shows a correction of the bitstream from "1101" to "1011" which is then detected at the collector [145]. **b** Top: Micromagnetic simulation results for a chain of skyrmions and chiral bobbers in the presence of a perpendicular magnetic field in a thin strip of FeGe. Bottom: Phase shift of an electron beam φ calculated for each configuration in the Top image. The phase shift can be detected by means of quantitative off-axis electron holography in a transmission electron microscope (TEM) [175]. **c** Top left: Diagram of ferromagnetic-antiferromagnetic (FM-AFM) bilayer device. Identical currents I_1 and I_2 serve as input signals to the AFM layer. Magnetic tunnel junctions (MTJs) A-D write the skyrmions and read the output voltage. Top center: MTJ spin configurations with the presence (top) and absence (bottom) of a skyrmion. Top right: Aerial view of MTJs (solid circles) and pinning centers (dashed circles). Bottom: Skyrmion motion in the FM layer under different current densities J and their resulting velocities v. The skyrmion motion (dashed arrows) deviates from the current direction (solid-colored arrows) due to the skyrmion Hall angle [181]. **d** Simulation results of various logic operations performed using the device structure in **c**. Skyrmions are positioned using pinning sites and move in response to applied input currents with trajectories indicated by the colored arrows [181].

drive skyrmions to move toward a racetrack boundary and finally lead to skyrmion annihilation. To address the issue of stability, skyrmions may be reliably positioned by using artificial defects. The pinning potential can also be designed to guide the skyrmion motion in a predictable manner [118].

Due to their metastable and non-dissipative properties, skyrmions have also been proposed in Boolean logic devices [176–183]. Skyrmion motion was first proposed in fixed logic devices (FLDs) in which the geometry is manufactured for a specific logic functionality [177–179]. This limits flexibility in applications as different geometries are needed for different logic functionalities. The successful operation of these FLDs relies on the skyrmion motion, skyrmion-skyrmion interaction, and interaction of skyrmions with geometric edges. More recently, several studies have proposed skyrmion-based programmable logic devices (PLDs) where multiple logic functionalities can be achieved in a single device [180–184]. Yan et al. exploited artificial defects to reliably guide and position skyrmions and achieved full logic functionality by choosing the input currents and initial position of skyrmions at different pinning sites (Fig. 3(c) and (d)) [181]. Currents I_1 and I_2 applied along orthogonal directions serve as inputs. The currents drive skyrmions to move from their initial pinning sites to other adjacent pinning sites. The existence or absence of a skyrmion in a selected position serves as an output. Different logic functions are conveniently achieved by choosing the initial states of the skyrmions (Fig. 3(d)). Luo et al. has demonstrated reconfigurable skyrmion logic devices by making use of the voltage-controlled magnetic anisotropy (VCMA) effect in selected regions of

the device [180]. Paikaray et al. manipulated local fields to control the trajectories of skyrmion motion and thereby realized reconfigurable logic operations [184]. Most of these research efforts are on simulation level and the physical implementation of these technologies may meet challenges in the precise control over skyrmion motion and in geometric and operational complexities.

Skyrmion motion driven by forces induced by magnetic fields, currents, voltages, and magnonic spin torques may also be utilized in the development of other computational devices as discussed below. In addition to these, the Brownian motion of skyrmions (Fig. 4(a)) [92,185–195] may also prove advantageous in applications. The force term **F** originating from the thermal effect should be uncorrelated in space and time, and therefore have an expectation value of zero, $\langle \mathbf{F}_{th} \rangle = 0$. Moreover, the variance should be proportional to the damping constant α and the temperature T, $\langle F_{th}^i(\mathbf{r}, t) F_{th}^j(\mathbf{r}', t') \rangle = 2\alpha k_B T \mathscr{D}_{i,j} \delta(\mathbf{r} - \mathbf{r}') \delta(t - t')$ [196]. This induces skyrmion diffusion with a mean squared displacement, $\mathrm{MSD}(\Delta t) = \langle [\mathbf{R}(t + \Delta t) - \mathbf{R}(t)]^2 \rangle = 4Dt$, where **R** is the position of a skyrmion and $D = k_B T \frac{1}{\mathscr{G}^2 + \alpha^2 (\mathscr{D}_{xx} \mathscr{D}_{yy} - \mathscr{D}_{xy}^2)} \begin{bmatrix} \alpha \mathscr{D}_{yy} & -\alpha \mathscr{D}_{xy} \\ -\alpha \mathscr{D}_{xy} & \alpha \mathscr{D}_{xx} \end{bmatrix}$. For a rotationally symmetric skyrmion, the diffusion constant can be simplified as $D = k_B T \frac{\alpha \mathscr{D}}{\mathscr{G}^2 + (\alpha \mathscr{D})^2}$ with $\mathscr{D}_{xx} = \mathscr{D}_{yy} = \mathscr{D}$ and $\mathscr{D}_{xy} = \mathscr{D}_{yx} = 0$. Skyrmion diffusion may become anisotropic with an elliptical deformation of the skyrmion configuration [194]. Note that, in real samples, the diffusion constant of a skyrmion may be nonlinearly dependent on temperature owing to
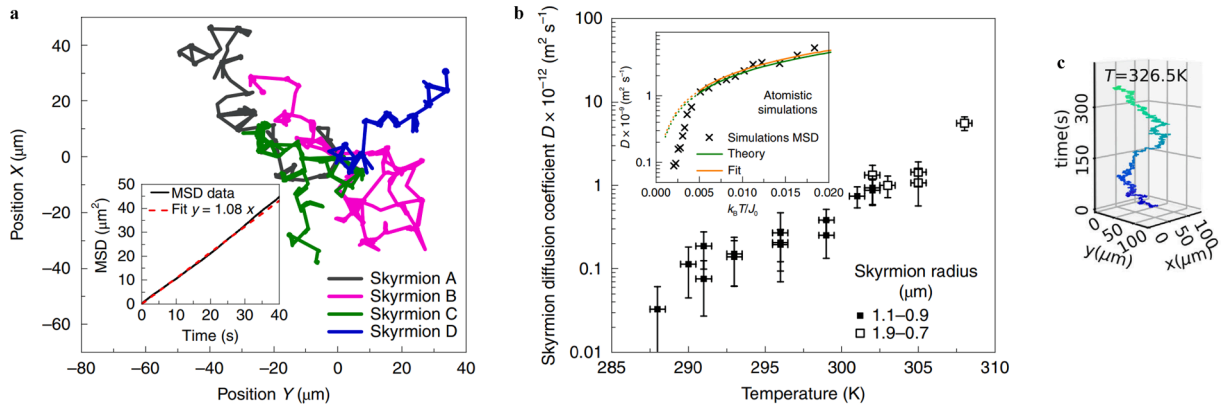
Fig. 4. **a** Position of four different skyrmions at room temperature in a low-pinning Ta/CoFeB/Ta/MgO/Ta multilayer measured using magneto-optic Kerr effect (MOKE) microscopy. The inset illustrates the time-averaged mean squared displacement (MSD) of the data [92]. **b** Semilogarithmic plots of the observed and simulation-based (inset) skyrmion diffusion constant as a function of temperature. Strong temperature dependence in the low temperature regime is predicted by the simulation, followed by quasi-free diffusion restored as the temperature is increased. Data points are averaged over measuring several skyrmions [92]. **c** Time-dependent trajectory of an isolated skyrmion with $Q = -1$ in a Ta/CoFeB/TaO$_x$ multilayer at 326.5 K. The Brownian gyromotion is observed [192].

pinning effects [92,186,193]. Zázvorka et al. [92], Nozaki et al. [186], and Goto et al. [193] have discovered exponential dependencies of the diffusion constant on the temperature (Fig. 4(b)), applied voltage, and AC magnetic field, respectively. This may be explained by the temperature, voltage, and field controls of thermally activated hopping diffusion where the escape time from pinning sites follows an Arrhenius' law and leads to this exponential dependence. More recently, Zhao et al. has experimentally observed topology-dependent Brownian gyromotion of skyrmions (Fig. 4(c)) [192]. This topology-dependent gyromotion can also be well described by the Thiele equation incorporating the thermal force. Brownian motion of skyrmions may provide new stochastic functionalities in applicational devices [92,188,195].

In addition to global translational motion, skyrmions, as particle-like entities, also possess a finite inertial mass and exhibit inertial dynamics [145,171,197–204]. These dynamics manifest themselves as the gyrating motion describing skyrmion motion in circular or spiral trajectories as well as the breathing mode, which describes the oscillatory variation in the skyrmion radius. These eigen excitations are in the Gigahertz regime and can be well described by the Thiele equation incorporating

the inertial term $\frac{\gamma_l}{M_s d} M \dot{v}$. These Gigahertz eigenmode dynamics have been observed in magnetic nanodisks [197] as well as in nanoribbons during skyrmion motion [145,171]. These eigenmode dynamics depend greatly on the applied fields and currents as well as the coupling between surrounding spin textures and geometric edges. Tomasello et al. has demonstrated that the breathing mode of skyrmions may set a limit on the maximum achievable velocity of skyrmion motion [171]. Additionally, Wang et al. has reported a coupling of the gyrating motion of a skyrmion to its breathing mode dynamics [145]. These inertial dynamic modes may provide new means to store information in practical systems.

Local dynamic properties of skyrmions. In addition to skyrmion motion, the successful implementation of skyrmionic devices requires functionalities with effective controls. Pinna et al. [205], Zhang et al [206], Yang et al [207], and Wang et al. [76] all have examined the local dynamics of skyrmions which may provide additional functionalities for versatile applications. Many of these research efforts make use of local defects to anchor part of the skyrmion while the other part exhibits a higher mobility and responds to the applied fields, currents, and thermal fluctuations. Pinna et al. has reported deformation of skyrmions under the
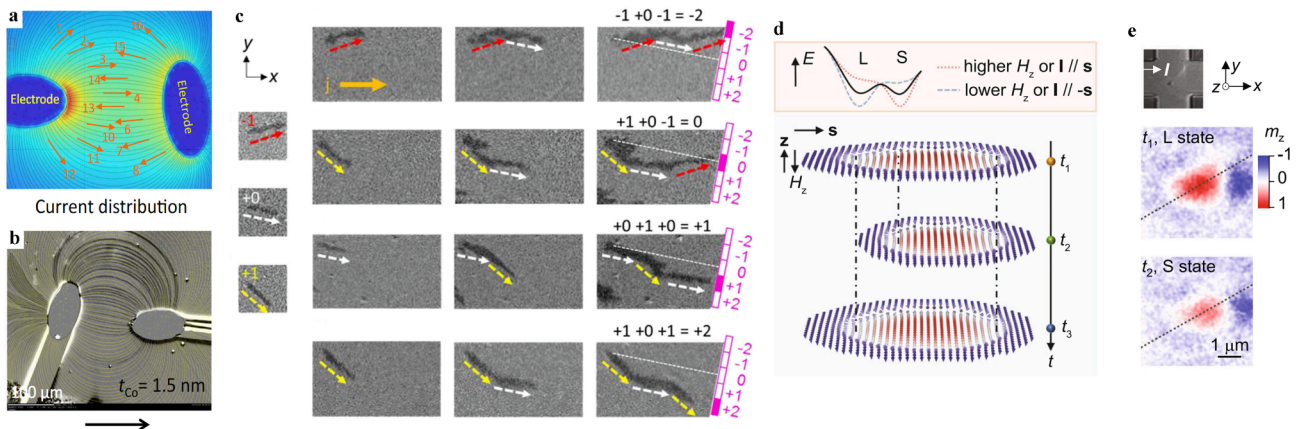
Fig. 5. Local dynamics of skyrmions. **a** Simulation of electric current distribution in a cobalt film using finite element modeling. **b** Emergence of magnetic strip domains in Ta/Pt/Co/Ta multilayer after applying a voltage pulse. Yellow lines indicate electric current distribution calculated in **a** [206]. **c** Addition operations achieved through chiral stripe domain elongation in W/CoFeB/MgO/Ta films in response to applied magnetic fields and current pulses. Each operation is carried out under a specific set of magnetic fields together with x-axis current pulses of 50 ms with a constant current density. The half-skyrmion exhibits distinct trajectories marked by red (+1), white (0), and yellow (-1) arrows under different sets of magnetic fields. The results of the operations, indicated by the termination of the stripe, are shown in pink [207]. **d** Schematic illustrating the fluctuation dynamics of skyrmions between large-skyrmion (L) and small-skyrmion (S) states over time as a result of interactions with local pinning centers. The energy barrier that exists between these two states, illustrated in the top panel, can be further tuned by the applied field and current. **e** MOKE images of an isolated skyrmion in the L and S states measured in a Ta/CoFeB/MgO/TaO$_x$ multilayer patterned into a Hall cross structure [76].

influence of applied currents [205]. The non-linear responses of the magnetization to currents may be utilized in the implementation of reservoir computing. Zhang et al. has used the trajectories of half-skyrmions under the influence of applied currents to map current distributions in space (Fig. 5(a) and (b)) [206]. Yang et al. has examined the magnetic field control of the half-skyrmion motion which may be relevant to adder/subtractor operations (Fig. 5(c)) [207]. In the adder/subtractor, each operation is carried out under a specific set of applied magnetic fields in conjunction with the x-axis current pulses. The half-skyrmion exhibits distinct trajectories marked by red (+1), white (0), and yellow (-1) arrows in Fig. 5(c) under different sets of magnetic fields. The results of the operations are indicated by the termination of the stripe.

More recently, Wang et al. has studied the skyrmion-size fluctuation in which one part of the skyrmion is more strongly pinned while the other part of the skyrmion, under thermal effects, fluctuates in time between two weaker pinning sites (Fig. 5(d)) [76]. This causes the skyrmion to exhibit thermal fluctuations between a small-skyrmion and a large-skyrmion configuration (Fig. 5(e)). This skyrmion-size fluctuation follows a purely random process and thereby promotes the skyrmion as a true random number generator (TRNG) for employment in cybersecurity, gambling theory, and scientific simulations. Wang et al. has also shown that neighboring skyrmions are linked by an anti-correlated coupling in their fluctuation dynamics in which one skyrmion has an increased probability at the large (small)-skyrmion state while the other skyrmion is at the small (large)-skyrmion state. This interaction is mediated by the demagnetization field. Both the fluctuation dynamics of a single skyrmion and the dynamic coupling strength between neighboring skyrmions can be tuned by the applied fields and currents. This offers a wide range of opportunities to implement systems based on either a single skyrmion or a skyrmion network with a high degree of tunability and controllability.

3. Electronic applications of skyrmions

These desirable properties of skyrmions have been proposed for use in numerous electronic applications in addition to skyrmion racetrack memory and logic devices. Examples include skyrmion transistors [208,209], skyrmion diodes [113], skyrmion spin-torque nano-oscillators (STNOs) [210–218], skyrmion neurons [219–228] and synapses [221,223,224,229–234] for neuromorphic computing devices, skyrmion reservoir computing devices [91,182,205,235–242], and skyrmion stochastic computing devices [76,91,92,188,191,195,243,244]. Zhang et al. [208] and Zhao et al. [209] have studied skyrmion transistors in which the likelihood of a skyrmion passing through the device is determined by the applied voltage through the VCMA effect. Zhang et al. has verified skyrmion STNOs that involve a skyrmion experiencing a circular motion in a nanopillar under an applied current with a vortex-like polarization [218]. In such applications, fundamental parameters include the working frequency, spectral linewidth, output power, and power consumption. These parameters are determined by the interplay of the current amplitude and edge potential as well as by the configuration of the detection electrode. The skyrmion motion in the nanopillar can be well described by the Thiele equation in Eq. (3) incorporating the current-driven force and edge potential. Compared to current mainstream STNOs which are generally based on the precession of the uniform magnetization [245] and vortex [246–252], skyrmion-based STNOs are characterized by a much lower current density required to excite the skyrmion motion, a broad working frequency, and a scalability. The output microwave signal may be detected by the MTJ-based STT diode with a high sensitivity. In this section, we will focus primarily on skyrmion neurons and synapses for use in neuromorphic computing devices, skyrmion reservoir computing devices, and skyrmion stochastic computing devices to address the issues of recognition, optimization, and invertible logic that von-Neumann computers fail to efficiently solve.

Skyrmion neurons and synapses for neuromorphic computing devices. It is well understood that neural arrangements of cortical visual networks are efficient in dealing with complicated tasks such as pattern recognition, language processing, disease prediction, and classification. Inspired from this, hardware implementations of deep neural networks have recently emerged and have drawn tremendous research attention. To implement neuromorphic circuits, it is necessary to develop artificial neurons and synapses which are two of the fundamental components in an artificial neural network (ANN). Numerous neurons are massively connected by synapses which transmit the neural signals between neurons (Fig. 6(a)). Although CMOS technologies have been used in the physical implementation of ANNs, CMOS-based ANNs have high spatial costs and are energy inefficient owing to the large number of transistors needed to model a spiking neuron and synapse [253–255]. Alternatively, post-CMOS technologies such as Ag-Si memristors [256], phase-change memories [257,258], and multilayer spintronic systems [259,260] are currently the focus of many research studies. Magnetic skyrmions are intriguing alternatives for hardware implementations of ANNs given their small size, high stability over time, and heightened immunity to material defects compared to other magnetic structures.

Artificial neurons are one of the fundamental components in ANNs and are employed to perform the nonlinear neuron activation function. One of the most widely accepted models describing neurons is the leaky-integrate-fire (LIF) model (Fig. 6(b) and (c)) [222,261–264]. This model describes how the ion current passes through the cell membrane, causing the membrane potential to increase and reach a certain threshold under a series of input current pulses I_{spk-in}. This is followed by a neuron spiking event which generates an output spike $I_{spk-out}$ and a subsequent reset process that repolarizes the membrane potential to its resting potential. The LIF model can be described and understood by [222,261,264].

$$\tau_{mem}\frac{dV}{dt} = -(V - V_{rest}) + \sum_j \delta(t - t_j)w_j. \tag{4}$$

In this equation, τ_{mem} is the decay time, V is the membrane potential, V_{rest} is the resting potential, and $\sum_j \delta(t - t_j)w_j$ is a sum of weighted input spikes. In skyrmion-based artificial neurons, current or voltage pulses may be used as input spikes. The membrane potential can be defined by the skyrmion position, skyrmion size, or other skyrmion characteristics.

Multiple skyrmion-based LIF spiking neuron concepts based on skyrmions have been proposed with most making use of the interactions of skyrmions with applied currents and geometric edges. Li et al. has designed a skyrmion-based artificial neuron by exploiting the current-driven skyrmion motion in a magnetic nanotrack with a linear variation in PMA (Fig. 6(d)) [226]. The potentials in Eq. (4) are denoted by the skyrmion position in the nanotrack. Current pulses drive a skyrmion to move across the nanotrack from the origin ($V_{rest} = 0$) to the targeted position to emit the output spike. The spatial variation in the PMA induces a nonuniform distribution of the energy U and thereby provides a driving force for the skyrmion to return to the origin, resulting in the reset of the skyrmion neuron. Chen et al. has also reported a skyrmion neuron in which the position of a skyrmion in the nanotrack defines the membrane potential (Fig. 6(e)) [222]. As the skyrmion moves along a nanotrack, which has a linear variation in its width, it encounters a force from the edge potentials that drives the device to reset. As discussed previously, the skyrmion Hall effect may limit the performance of many skyrmion-based devices. This effect may be eliminated in spiking neurons by antiferromagnetic skyrmions in antiferromagnetically exchange-coupled magnetic systems [223].

The spiking neuron has also been modeled by skyrmions using inter-skyrmion repulsion [220], skyrmion distortion under external stimuli [219,227], and skyrmion STNO behavior [228]. Bindal et al. has proposed a device consisting of a magnetic anisotropy barrier on a nanotrack in which the integrate-fire functionality is achieved by exploiting inter-skyrmion repulsion [220]. The membrane potential in Eq. (4) is
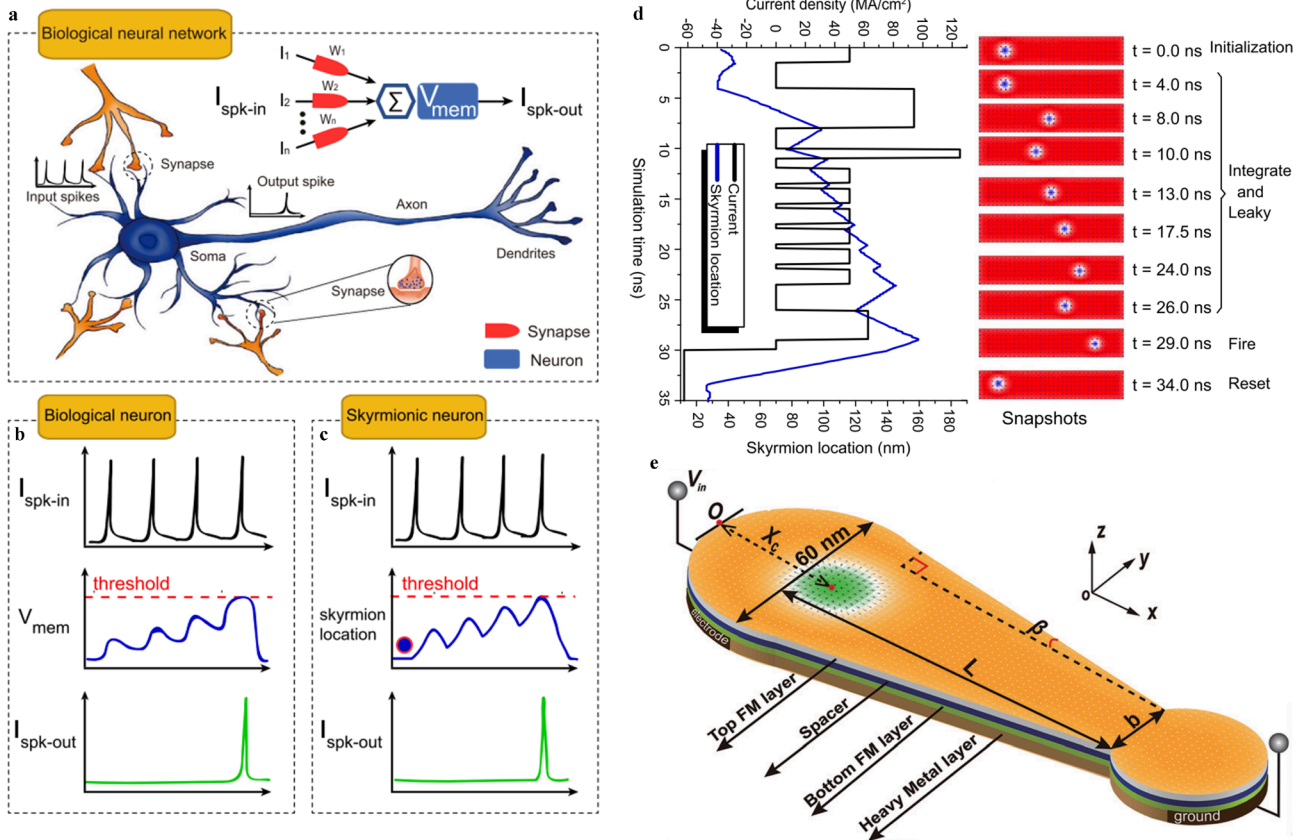
Fig. 6. a Drawing of a biological neural network along with a schematic of the basic operation that consists of input spike currents I_{spk-in}, synaptic weights W, sum of membrane potentials V_{mem}, and output spikes $I_{spk-out}$ [226]. **b** and **c** illustrate the leaky-integrate-fire (LIF) spike neuron concept for the cases of the biological neuron and the skyrmion-based neuron, respectively [226]. **d** Micromagnetic simulation results for an inhomogeneous input spike current. The skyrmion motion is shown in a track with linearly increasing perpendicular magnetic anisotropy (PMA) from left to right, as opposed to a constant PMA, that exhibits "leaky-integrate" behavior. The skyrmion moves from left to right by current pulses and move backwards in the absence of a current due to the force induced by the anisotropy gradient [226]. **e** Diagram of skyrmionic LIF spiking neuron device. The input spikes, which are applied to the V_{in} terminal, manipulate the skyrmions in the central region where the width varies linearly. The membrane potential can be determined from the distance of the skyrmion core to the base point, O, and is defined as X_c here. Once this passes a threshold, an output spike is generated. The skyrmions can optionally be detected in the circular region at the right end of the device [222].

denoted by the number of skyrmions pinned by the barrier. Once the skyrmion number reaches a threshold, a skyrmion overcomes the barrier owing to the inter-skyrmion repulsion and emits the output spike. Azam et al. [219] and Zhu et al. [227] have reported spiking neurons using the

voltage control of PMA and voltage-generated strain as input signals to control the skyrmion size (Fig. 7(a)) which, along with the resistance signal, acts as the membrane potential. Azam et al. has also designed a CMOS buffer circuit in which the output spike is produced by turning on
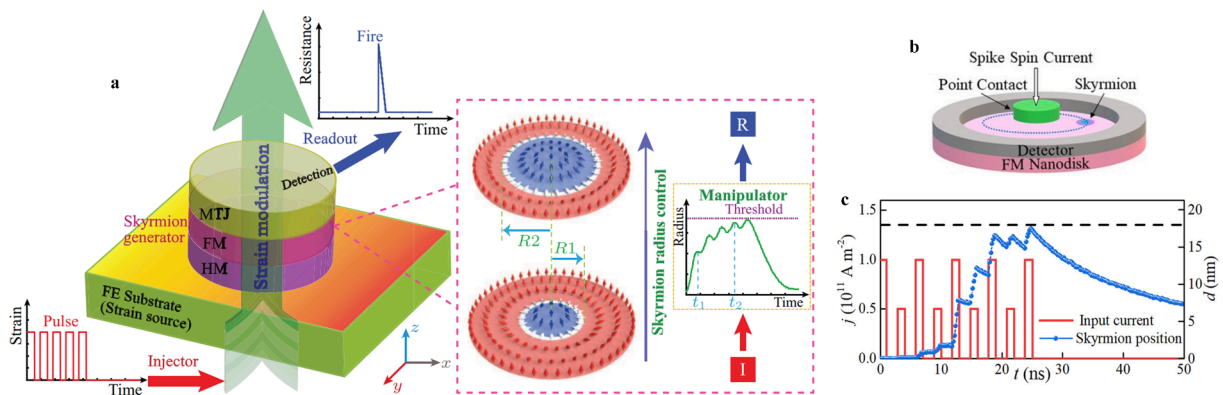
Fig. 7. a Illustration of a spiking neuron device that consists of a skyrmion generator, a magnetic tunnel junction (MTJ) detector, and an external strain source with pulsed modulation. Schematic of the variation in the skyrmion radius over time is illustrated in the inset. The skyrmion size increases under voltage pulses due to the modification of the PMA and returns back to its original size in the presence of the bias voltage [227]. **b** Schematic of a skyrmion-based spiking neuron consisting of a nanoscale point-contact, a skyrmion-based spin-torque nano-oscillator (STNO) and a ring-shaped electrode [228]. **c** Time-dependent skyrmion position under the influence of a nonuniform square wave spike current with frequency of 0.5 GHz. The current is applied through the center nanorod and flows radially towards the ring-shaped electrode. The radial distribution of the current causes the skyrmion to move circularly such that the radius of motion serves as the membrane potential [228].

the transistor when the electrical resistance decreases to a threshold [219]. Liang et al. has constructed a spiking neuron using a skyrmion-based STNO where the current pulses are the input spikes introduced from a point nanocontact at the nanopillar center. The radius of skyrmion motion serves as the membrane potential (Fig. 7(b) and (c)) [228]. In this design, the skyrmion neuron generates the output spike when the radius of motion reaches a threshold, after which the neuron is reset with the force from the edge potential driving the skyrmion back to the origin.

The spikes emitted by pre-neurons propagate through synapses to the post-neurons and are modulated with synaptic weights during the spike transmission process (Fig. 6(a)). There are two different types of synapses in biological systems: electrical and chemical [265]. Electrical synapses transfer electrical charges from pre-neurons to post-neurons via ions that travel through gap junctions between cells while chemical synapses transform signals through the release of chemicals called neurotransmitters. In biological systems, synaptic plasticity is essential to the modulation of synaptic weights and thereby to the processes of

remembering and forgetting. Synaptic plasticity includes the short-term plasticity (STP) that describes the temporal enhancement of the weight followed by a quick decay as well as the long-term potentiation (LTP) marked by a permanent change caused by repeated stimulation. Artificial synapses must accommodate for the synaptic plasticity together with the temporal dynamics to accurately mimic biological synapses.

Multiple designs for skyrmion synapses have been proposed with the synaptic plasticity relying on either the number of skyrmions in a specific region [221,223,229–234] or on the skyrmion size [266,267]. This allows for modulation of the synaptic weight represented by the conductance measured using the TMR effect or with anomalous Hall detections. Huang et al. have proposed a skyrmion synapse based on skyrmion motion in a track with a rounded, rectangular barrier in-between the pre-synapse and post-synapse regions (Fig. 8(a) and (b)) [232]. In this model, the skyrmions move from the pre-synapse to the post-synapse region under the influence of current pulses that serve as stimuli from the pre-neurons. If the input stimuli are not sufficient, the skyrmions may approach the barrier and retreat under the repulsive
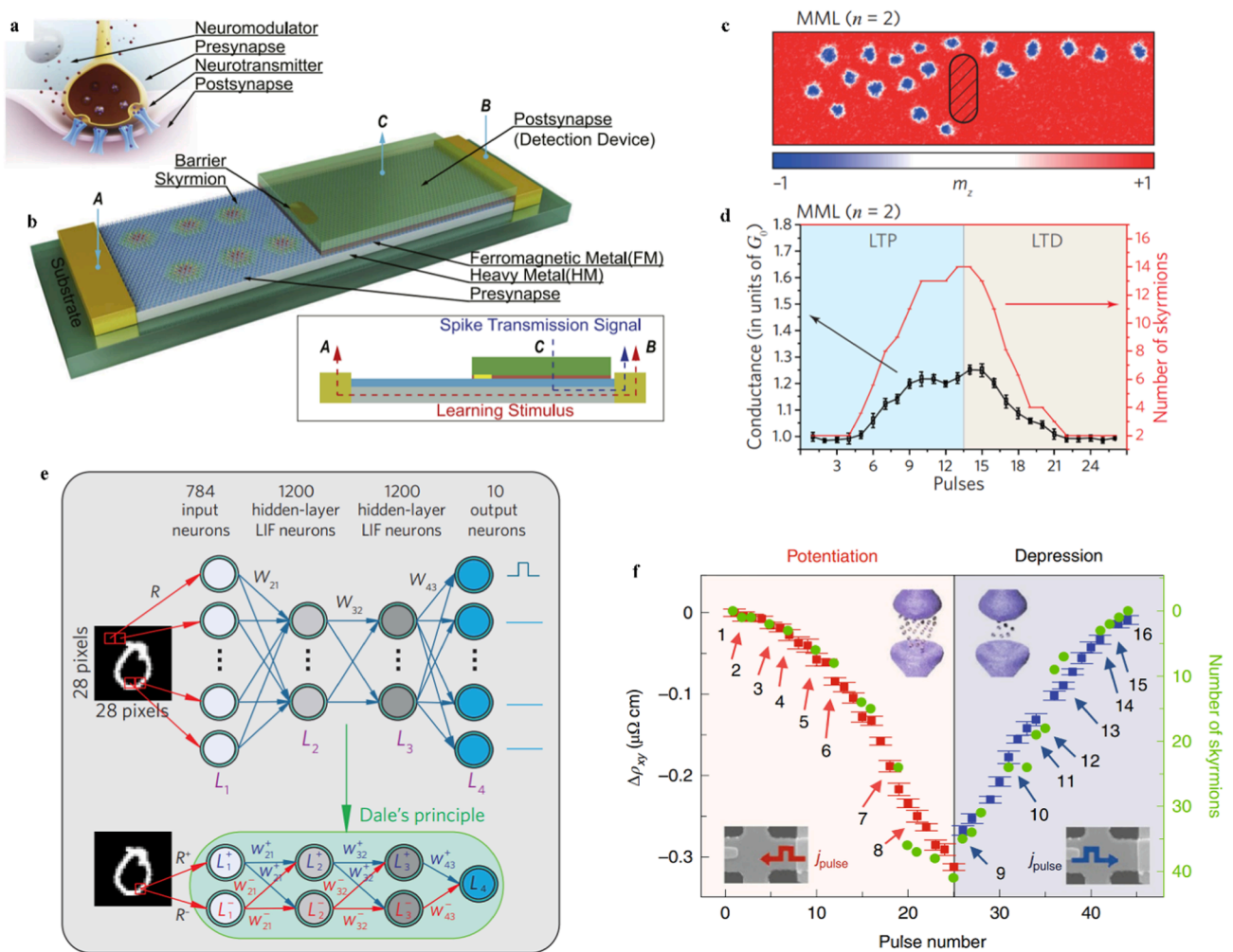
Fig. 8. a Illustration of biological synapse with relevant parts labeled [232]. b Design of a skyrmion synapse. Neuromodulator is modeled by a learning stimulus that passes through the heavy-metal (HM) layer from terminal A to B. This stimulus can either drive the skyrmions into the post-synapse region, in which case the synaptic weight increases, or back into the presynaptic region, by which the synaptic weight would decrease. This resembles the biological processes of potentiation and depression, respectively. Terminal C measures the synaptic weight [232]. c Results of micromagnetic simulations of a skyrmion synapse with colors representing the direction of magnetization in a $[HM/FM/HM]_n$ stack at room temperature (where $n = 2$). The rounded rectangular barrier is illustrated, separating the pre- and postsynaptic regions [231]. d Plot showing the variation in conductance of the sample (black data) relative to the number of skyrmions in the post-synapse region (red data) [231]. e Schematic of skyrmion-based deep ANN including input neurons, two sets of hidden-layer LIF neurons, output neurons, and synaptic weights (W_{ij}) used to learn the handwritten pattern provided as input [231]. f Measured Hall resistivity change and calculated skyrmion number as a function of injected pulse number in $[Pt (3 \, nm)/Gd_{24}Fe_{66.6}Co_{9.4} (9 \, nm)/MgO (1 \, nm)]_{20}$ ferrimagnetic multilayer stacks. The red/blue symbols and colored areas correspond to resistivity changes (left axis) during potentiation and depression, respectively. Green symbols indicate the number of skyrmions (right axis). Insets illustrate the direction of charge current pulses [234].

force from the barrier, leading to the STP. Skyrmions may also pass through the barrier, leading to the LTP, if stimuli are sufficient in duration and/or frequency. The synaptic weight resolution is determined by the maximum number of skyrmions in the post-synapse region. In turn, applying negative stimuli may lead to the depression of the skyrmion synapse. Huang et al. has also determined that there are trade-offs between the synaptic weight resolution, processing speed, functional area, and energy consumption. These parameters are governed by the track geometry and the barrier design. Although the simulation study illustrates the successful operation of the skyrmion synapse at zero temperature, the synapse may fail at room temperature owing to fluctuations in the shape of skyrmions. The stability of skyrmions at room temperature may be increased along with a reduced standard deviation of the conductance, by fabricating magnetic multilayers with repeating heavy-metal/magnetic/heavy-metal layer structures (Fig. 8(c) and (d) for the repetition $n = 2$ of the multilayer structure) [231]. The energy consumption per synaptic update event is estimated to be about 300 fJ. The functionality of room-temperature skyrmion synapses was validated by simulating a two-layer unsupervised ANN and a supervised deep ANN (Fig. 8(e)) on the Modified National Institute of Standards and Technology (MNIST) handwritten digit data set using BRIAN, a Python-based simulator [231]. This aims to achieve superior accuracy in pattern recognition tasks. In simulations, synapses are embedded into a crossbar array to provide the synaptic weights connecting two layers of neurons which are implemented by analog circuits. Chen et al. has achieved approximately 78 % classification accuracy by using a two-layer unsupervised ANN and approximately 98.61 % accuracy by using a deep ANN with supervised learning, suggesting that room-temperature skyrmion synapses hold great promise for future energy-efficient neuromorphic computing [231]. In 2020, Song et al. experimentally reported the potentiation and depression behaviors of a skyrmion synapse in a Pt/GdFeCo/MgO multilayer where the accumulation and dissipation of skyrmions is controlled by electrical current pulses (Fig. 8(f)) [234]. The synaptic weight is modeled by the anomalous Hall conductance. Song et al. has also simulated a deep ANN based on the synaptic weights obtained experimentally with the aim to learn the MNIST handwritten pattern data set and to perform pattern recognition. Simulation results have yielded a recognition accuracy of about 89 % which is comparable to the roughly 93 % accuracy of software-based ideal training.

In addition to current-driven accumulation and dissipation of skyrmions, surface acoustic waves [230] and ultrafast lasers [233] have also been demonstrated to be effective in tuning the number of skyrmions in the post-synapse regions. In addition, Chen et al. has reported skyrmion synapses by using a set of *N*-number skyrmion devices. The existence or absence of a skyrmion in the detection region of each branch yields a distinct synaptic conductance [221]. This leads to 2^N discrete conductance states serving as synaptic weights. Luo et al. [267] and Yu et al. [266] have proposed skyrmion synapses with a variable skyrmion size which can be manipulated by the VCMA effect and/or the voltage-induced strain. The remnant strain helps to stabilize the skyrmion size and achieve synaptic plasticity.

The effective controllability of skyrmions together with their small size and stability promotes them as promising candidates for neurons and synapses in neuromorphic computing applications. Although multiple studies have verified the viability of skyrmion neurons and synapses, there exists a gap in the integration between these two components that is necessary to realizing all-skyrmion neuromorphic computing devices.

Skyrmion stochastic computing devices. Stochastic computing is an unconventional computing scheme that utilizes streams of random bits in addition to simple bitwise operations performed on the streams. A stream of bits, typically denoted by entities that fluctuate in time between "0″ and "1", may interact with other streams via neural network-inspired principles. Stochastic computing has been demonstrated to be efficient in solving a wide range of optimization problems such as probabilistic inference, sampling, invertible logic, and integer

factorization [45–49,268,269]. Multiple systems have been proposed for stochastic computing including CMOS technologies [270], trapped ions [271], electromechanics [272], optics [273–275], and magnetic systems [45–49,268,269,276–278]. Most of these systems exploit phenomena that are naturally probabilistic. A well-known example is the stochastic MTJ [45–49,268,269] in which the energy barrier for magnetization reversal in the free layer is small relative to the thermal energy. This leads to a stochastic magnetization configuration and thereby thermal fluctuations of the TMR in time between two discrete states (Fig. 9(a) and (b)). A resistor with the resistance R_{SOURCE} and an NMOS transistor were used to restrict the current through the stochastics MTJ. A comparator leads the output signals to be either ideal "0" or "1". Camsari et al. [45] and Borders et al. [49] have examined the capability of a network of stochastic MTJs in solving the dilemmas of invertible logic and integer factorization. In the circuit, Borders et al. used an Arduino microcontroller to read the output signals and implement the synaptic weights. A data acquisition (DAQ) system was then used to communicate with the microcontroller and convert the results into analog voltages which were then sent back to NMOS (Fig. 9(c)). Borders et al. has successfully demonstrated the integer factorization by using 8 stochastic MTJs as well as the invertible AND gate operation (Fig. 9(d)) [49]. Kaiser et al. has developed an operating circuit using stochastic MTJs to perform hardware-aware machine learning for optimization tasks [48]. The weights were updated autonomously by using a RC network which models the Boltzmann-machine learning algorithm (Fig. 9(e)). This can counter device-to-device variations and perform operations such as learning of a full adder. Hayakawa et al. has obtained that the relaxation time of a stochastic in-plane easy-axis MTJ can be reduced down to 8 ns (Fig. 9(f) and (g)) [46]. A short relaxation time benefits stochastic computing with fast operation speed.

The inherent stochastic properties underlying the Brownian motion and internal fluctuations of skyrmions also promote them as intriguing candidates for stochastic computing. Yao et al. has proposed, through micromagnetic simulations, a skyrmion TRNG utilizing the Brownian motion of a skyrmion in a magnetic thin film (Fig. 10(a) and (b)) [191]. In this model, the skyrmion diffuses randomly in the magnetic thin film and its position, either in the right or left-hand side of the device, is used to encode the bit. Two MTJs were proposed for signal detection. In a magnetic thin film with uniform material parameters, the probability of the skyrmion being on either side is about 50 % (Fig. 10(b)). The probability can be tuned by introducing a lateral asymmetry (e.g., by adding an anisotropy gradient through the VCMA effect). Medlej et al. has also suggested through simulations a skyrmion TRNG by exploiting the skyrmion motion in a synthetic antiferromagnet [244]. Antiferromagnetic skyrmions are not affected by the skyrmion Hall effect. A skyrmion enters from an input branch into either one of the two output branches, leading to the generation of bitstreams with probabilities of approximately 50 % (Fig. 10(c)). Ishikawa et al. has experimentally implemented a skyrmion cellular automaton in which two adjacent cells were fabricated with each cell hosting two skyrmions (Fig. 10(d) and (e)) [195]. The two-skyrmion arrangement in each cell can be converted to a binary state based on their relative positions which are governed by Brownian motion of skyrmions and the dipolar interaction (Fig. 10(f)). In each cell, the two skyrmions occupy diagonal positions due to the dipolar interaction. In addition, the two skyrmions closest to the gap are anticorrelated in their positions such that when the skyrmion in the left cell is displaced downward or upward, the skyrmion in the right cell is displaced upward or downward, respectively (Fig. 10(f)). Difficulties in the implementation of such skyrmion-based devices include the unintended effects of edge roughness and local defects on skyrmion motion as well as the integration of MTJs with the device for signal reading and processing.

More recently, Wang et al. has experimentally verified a single-skyrmion TRNG based on the local dynamics of an isolated skyrmion (Fig. 5(d) and (e) and Fig. 10(g) – (i)) [76]. A single skyrmion is held in place by local pinning centers and fluctuates randomly in size between
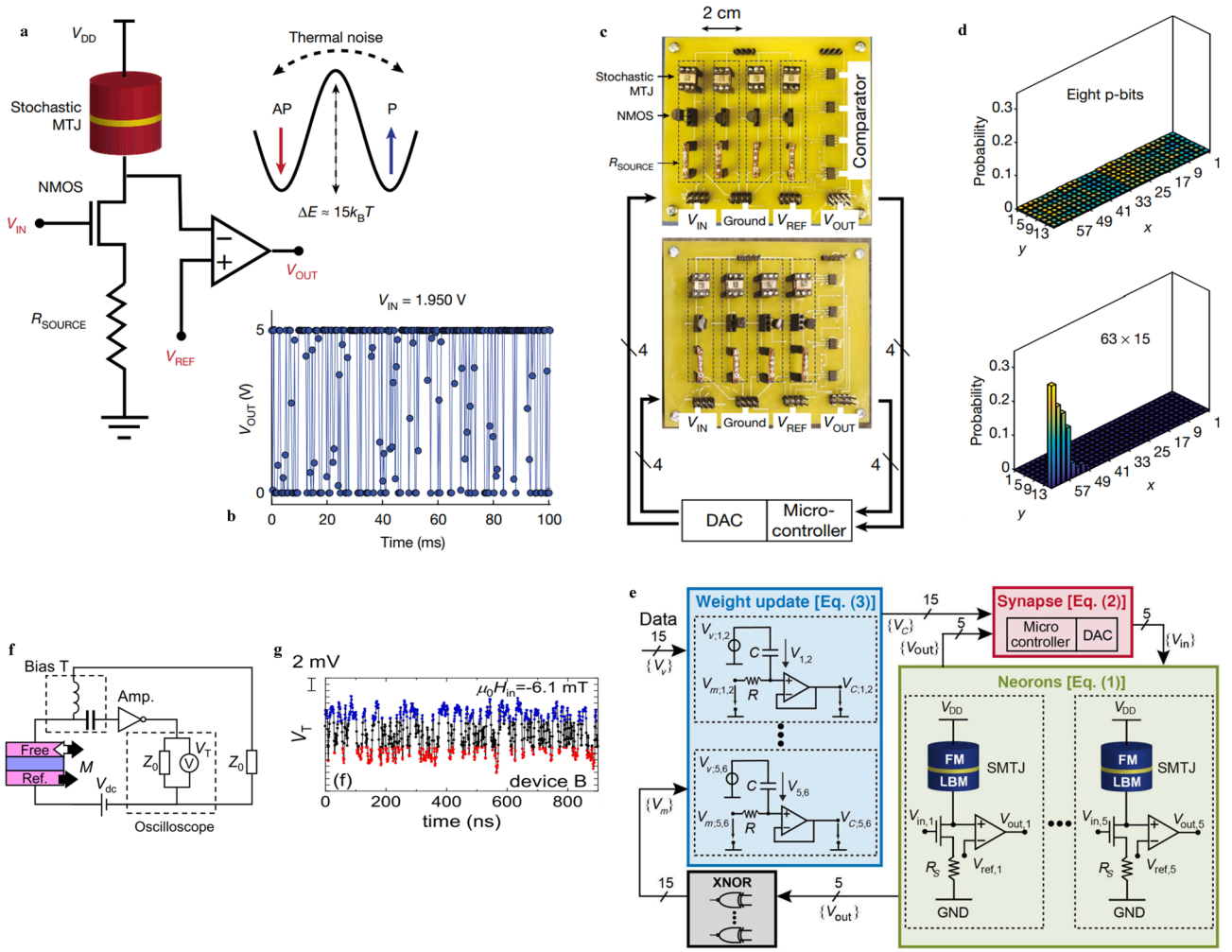
Fig. 9. a A probabilistic bit formed by a stochastic magnetic tunnel junction (MTJ) with a resistor, an NMOS transistor and a comparator. The energy profile between the parallel (P) and antiparallel (AP) states of the magnetization orientation of the stochastic MTJ is also shown [49]. **b** Time snapshots of the output signal V_{OUT} from the comparator for the input $V_{IN} = 1.950$ V, showing the fluctuation of the tunneling magnetoresistance induced by the fluctuation of the MTJ magnetization [49]. **c** A photograph of a probabilistic circuit composed of 8 stochastic MTJs. A microcontroller and a data acquisition (DAC) are interconnected for signal readout and weight implementation [49]. **d** The uncorrelated (top) and correlated (bottom) state of the circuit for integer factorization of $945 = 63 \times 15$. More than 2,000 sampling points are collected for statistics [49]. **e** Block diagram of the probabilistic learning circuit. $\{V_{in}\}$ are input voltages to NMOS. $\{V_{out}\}$ are output voltages from comparators. $\{V_{ij}\}$ are weight voltages. $\{V_C\}$ are capacitor voltages. $\{V_m\}$ are correlation voltages between probabilistic MTJs. $\{V_v\}$ are data distribution correlation voltages. The RC network was used to model the Boltzmann-machine learning algorithm [48]. **f** Circuit configuration of the random telegraph noise (RTN) measurements of an in-plane MTJ [46]. **g** Time snapshots of the output signal V_T, showing a relaxation time of 8 ns of the in-plane MTJ [46].

two discrete states (Fig. 5(d)). The skyrmion size fluctuation has been observed through both direct magnetic imaging (Fig. 5(e)) and Hall-resistivity measurements (Fig. 10(g)). The switching probability of the skyrmion can be tuned by modifying the applied field (Fig. 10(h)) and current (Fig. 10(i)) owing to the Zeeman-energy variation and SOT, respectively. The switching probability can be tuned from 0 to 1 even when the field is changed by an amount as small as 0.3 Oe (Fig. 10(h)) or when the current is changed by an amount as small as 0.25 mA (Fig. 10 (i)). Wang et al. has also examined the fluctuation rate of a skyrmion which may increase with elevating the temperature T, reducing the energy barrier ΔE, and reducing the distance between two weaker pinning sites. The fluctuation rate of a skyrmion can reach 10 MHz or even higher by manipulating the distribution of artificial defects. This may be realized by thickness modulations as well as by embedded impurity atoms and adatoms formed by advanced thin film fabrication, lithography, irradiation, and ion implantation techniques. Compared to other stochastic neurons, skyrmions exhibit intriguing features including high mobility in magnetic systems, reversible polarity, and mutual interactions that advocate skyrmion networks for

implementation in devices. Low electronic signals of skyrmions may be further enhanced by reducing the active detecting area relative to the skyrmion size.

Stochastic computing is established by operations on streams of random bits. The driving principle is that every bit of one stream interacts with every bit of the other stream. One example is an AND-gate implementation of the multiplication operation. The output generates a bitstream with the probability of pq with two uncorrelated input streams with probabilities of p and q respectively. The accuracy is ensured by observing a sufficient number of output bits. Zhang et al. has suggested by simulations AND logic as a multiplier for two streams of skyrmions where the presence or absence of a skyrmion is encoded as a "1″ or "0" (Fig. 11(a) and (b)) [243]. In the logic device, two electrode gates with voltages V_{g1} and V_{g2} are designed to modulate skyrmion motion through the VCMA effect. When a gate voltage is applied, an energy barrier is created in the gate region and skyrmions are blocked from crossing the region. When the voltage is turned off, skyrmions are allowed to cross the gate. When either input generates a skyrmion, corresponding to "1", and the other input generates the code "0", the skyrmion always goes
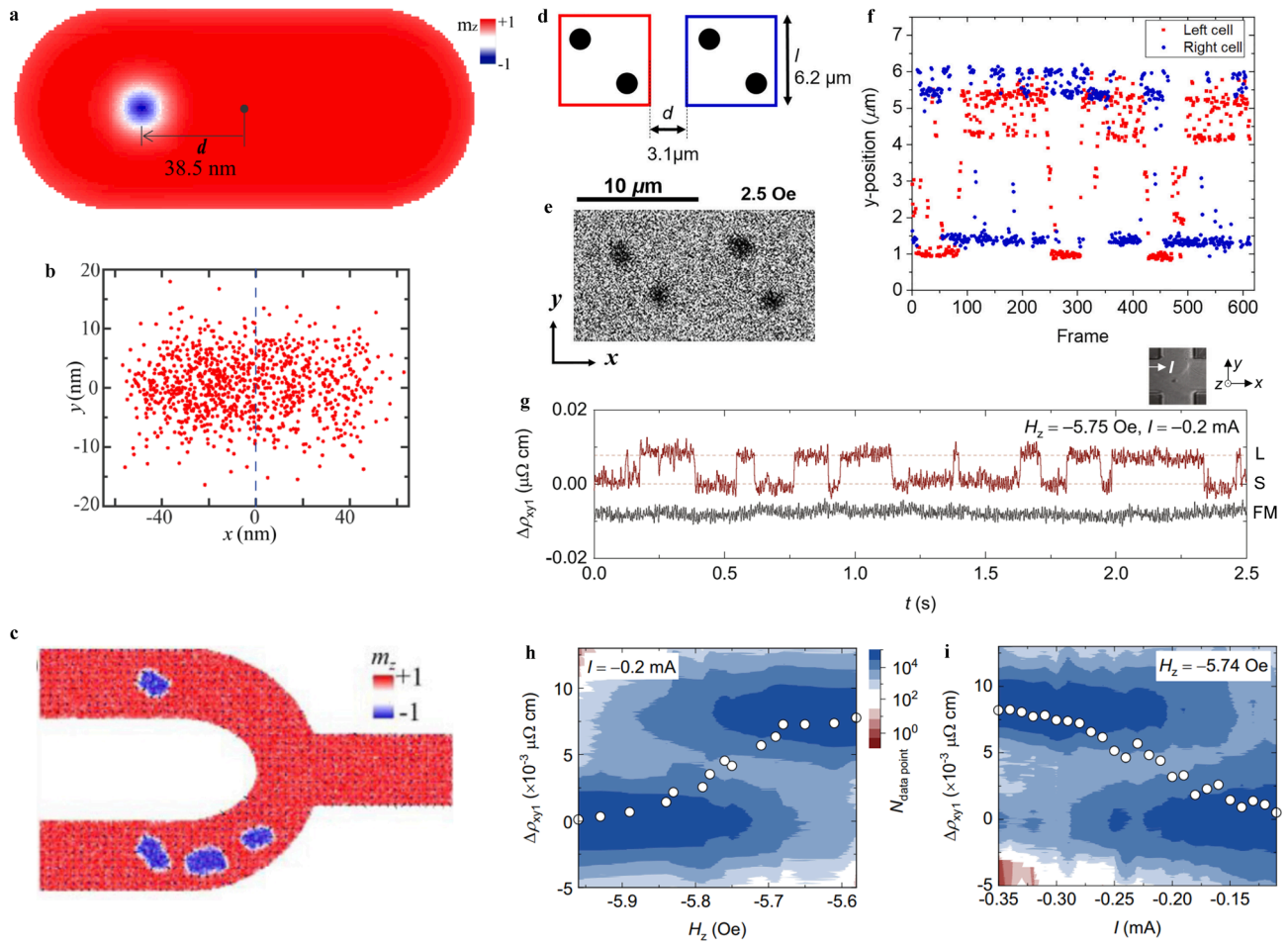
Fig. 10. a Top view of a true random number generator (TRNG) device based on the Brownian motion of a skyrmion with magnetization configuration of the m_z component in a heavy-metal/ferromagnetic (HM/FM) multilayer stack [191]. **b** Scatter plot of skyrmion position over a time interval of 1000 ns with 1 ns between consecutive data points [191]. **c** Top view of a TRNG device based on antiferromagnetic skyrmions [244]. **d** Schematic and **e** MOKE images of a skyrmion cellular automaton consisting of two adjacent square cells, each hosting two skyrmions [195]. **f** Time-dependent position of the two skyrmions closest to the gap, one in each of the red and blue cells [195]. **g** Inset: a TRNG device using the local dynamics of a skyrmion with the Hall cross as a transducer for signal readout and processing. The relative Hall-resistivity $\Delta\rho_{xy}$ fluctuates in time between $\Delta\rho_{xy} \approx 0$ and $\Delta\rho_{xy} \approx 0.008\mu\Omega\,cm$ for a single skyrmion. This corresponds to a skyrmion-size fluctuation between the small (S)-skyrmion and large (L)-skyrmion configuration. The signal for a saturated ferromagnetic (FM) state is also shown [76]. **h** Density of data points for the $\Delta\rho_{xy}$ as a function of an applied field H_z at a fixed applied current of $I = -0.2$ mA. White dots represent time-averaged resistivities. [76]. **i** Density of data points for the $\Delta\rho_{xy}$ as a function of applied current I at a constant magnetic field of $H_z = -5.74$ Oe [76].

into the OR-output end of the device. This is due to the influence of the wedge-shaped geometry on the skyrmion motion [243]. In this case, the OR-output end reads "1" and the AND-output end of the device read "0". On the other hand, when both inputs generate skyrmions, skyrmion motion is also affected by the skyrmion-skyrmion repulsion and the two skyrmions go into the OR-output end and AND-output end, separately, with both output ends reading "1". By this, one can achieve the multiplication function for two random bitstreams of skyrmions (Fig. 11(a) and (b)) [243].

Zhang et al. has also replicated a multiplexer device as a stochastic adder [243] in which two input streams of skyrmion bits are selected by a signal with a probability of 0.5. This leads to an output bitstream with a probability of $0.5(p+q)$. These device operations also rely on manipulation of the skyrmion motion via the VCMA effect with voltages applied in some specific regions of the device.

Note that the operations may fail if correlations exist between the two input signals. This may be resolved by adding a reshuffler device which can convert a bitstream into an uncorrelated signal (Fig. 11(c)). Pinna et al. has proposed a reshuffler device exploiting Brownian motion of skyrmions [91]. Input and output signals are denoted by the skyrmion states at the input and output ends. Skyrmions move from the input end

to the output end in the presence of an applied current in addition to their intrinsic thermal diffusion at elevated temperatures. This leads to a rearrangement of skyrmions at the output end and gives rise to a signal that is uncorrelated to that of entry. Zázvorka et al. has experimentally fabricated such a reshuffler device in a magnetic thin film of Ta/ $Co_{20}Fe_{60}B_{20}$/Ta/MgO/Ta (Fig. 11(d)) [92]. The need for a reshuffler device, however, is eliminated by implementing random bit generators at the input ends. Successful demonstrations of the viability of skyrmion random bit generators are needed in performing optimization tasks.

Skyrmion reservoir computing devices. Reservoir computing is a recurrent neural network (RNN) based framework for temporal information processing [279]. This is distinct from feedforward neural network (FNN) which is suitable for static, i.e., non-temporal, data processing. Reservoir computing is a unified framework derived from independent RNN models including echo state networks and liquid state machines. It includes an input layer, a reservoir, and an output layer (Fig. 12(a) and (b)). Inputs are spatiotemporal patterns transformed from input data while the reservoir is used for nonlinear mapping of input signals onto a high-dimensional space. The one-dimensional readout in the output layer can be trained to extract features of the inputs for categorization. Reservoir computing does not require any
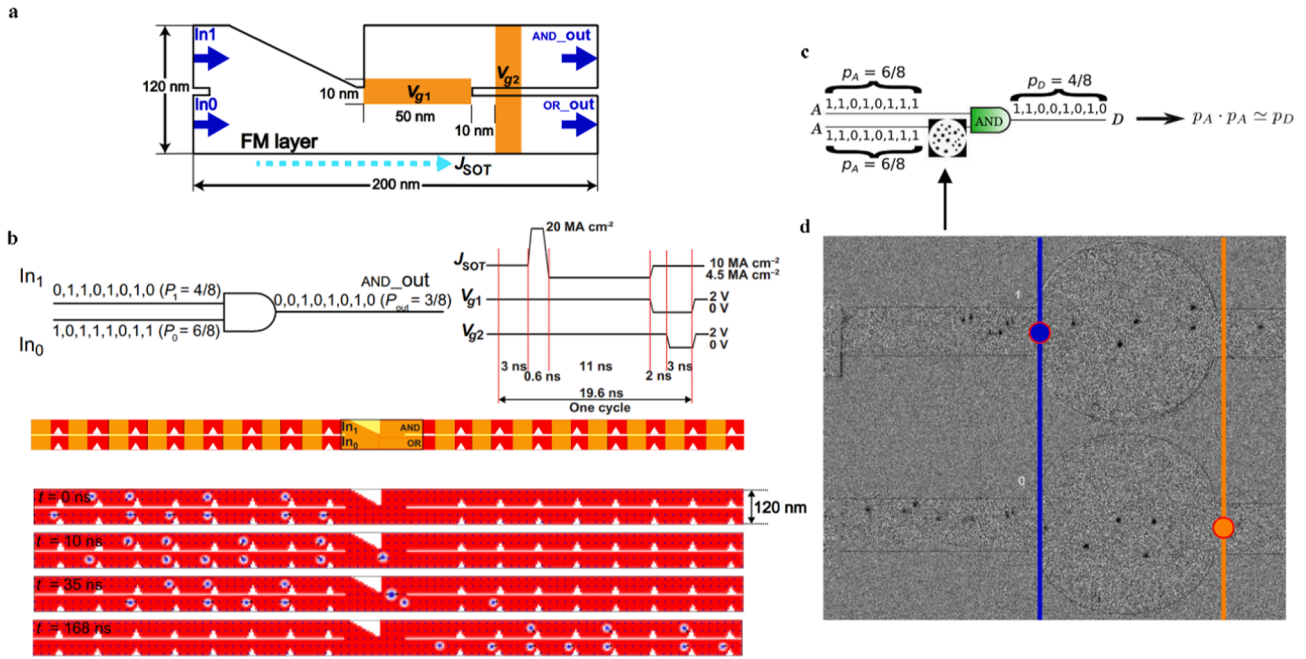
Fig. 11. a Skyrmion-based AND/OR logic gates with two input and output tracks. The electrode gates V_{g1} and V_{g2} are used to control skyrmion motion by the VCMA effect [243]. **b** Top left: Multiplication operation using AND gate. Top right: Contour of driving current density and electrode voltages over one cycle. Center: Schematic of skyrmion stochastic multiplier. The white notches separate the top and bottom tracks into eight regions. Bottom: Magnetization configuration of schematic in center diagram at various timestamps. At $t = 0$ ns, the input probabilities are *4/8* and *6/8* in the top input and bottom input tracks, respectively. After the application of a current density, the AND track correctly yields the multiplied probability of *3/8*, or "00101010" as a binary sequence [243]. **c** Schematic of a stochastic computing device using AND gate. One input signal is first reshuffled using the reshuffler device in **d** and becomes uncorrelated while retaining the same probability values [91]. **d** Skyrmion reshuffler device operation in a $Pt_{95}Ir_5/Fe/Pd$ thin film. Skyrmions are nucleated by applied currents and their motion across the blue and orange lines dictates the input and output signals, respectively, in terms of bits "0" and "1" [92].
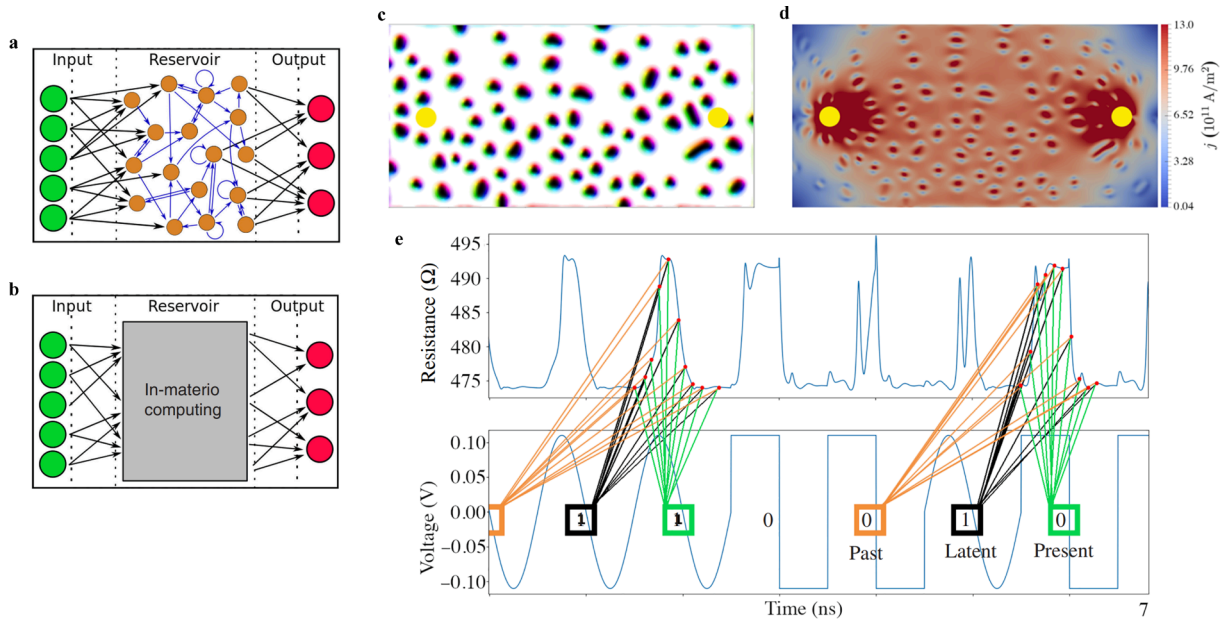
Fig. 12. Schematics of **a** a recurrent neural network and **b** a material-based reservoir [205]. **c** Simulation of skyrmion reservoir. Locations of green and red circles refer to input and output contacts, respectively [205]. **d** Current density distribution across the skyrmion network shown in **c** after application of a voltage to the electrical nanocontacts represented by the yellow circles [205]. **e** Illustration of time-dependent training and operation of the output layer. The measured resistance values are summed by three different weights trained for recognizing either the present pulse, the latent pulse, or the past pulse [205].

knowledge of the weights of recurrent connections within the reservoir for training purposes. Only the output weights are needed for training. This meets the demands for low energy consumption and training simplicity in applications. Reservoir computing has been demonstrated to be effective in solving a wide range of tasks including pattern

classification [280–283], time series forecasting [284,285], pattern generation [286,287], adaptive filtering and control [288], system approximation [289], and short-term memory [290]. Reservoir computing can utilize the naturally existing networks in physical systems since node weights in the reservoir are not trained. Various

physical systems such as electronic circuits and devices [291,292], photonics [293], magnetic [294], and mechanical systems [295] have been proposed for reservoir computing. Systems for reservoir computing applications must possess properties of sufficient nonlinear dynamics and short-term memory.

Magnetic skyrmions are suitable for realizing reservoir computing owing to the self-organization emergence of skyrmion lattices or fabrics in magnetic systems along with their nonlinear responses to external stimuli. Prychynenko et al. [240], Bourianoff et al. [235], and Pinna et al. [205] have all presented, through simulations, skyrmion reservoir computing devices by exploiting non-linear voltage responses of skyrmion fabrics to applied currents. The nonlinear current–voltage characteristics arise from the distortion of skyrmions interacting with local pinning centers along with the variable magnetization and magnetoresistive effects. Prychynenko et al. [240] and Bourianoff et al. [235] have analyzed the responses of a single skyrmion and skyrmion fabrics, respectively, to the current flow as well as the pinning effect on skyrmion dynamics. Pinna et al. has examined the employment of skyrmion fabrics for identifying and characterizing feature correlations of input voltage patterns (Fig. 12(c) – (e)) [205]. This operation exploits the fading memory functionality of the system by which the magnetization dynamics become highly sensitive to both the instantaneous driving current intensity and the memory of past voltage pulses. These simulation studies were performed at zero temperature. Major concerns regarding the implementation of such devices pertain to the thermal fluctuations and low signals associated with magnetoresistive effects.

Rajib et al. has proposed, by simulations, room-temperature skyrmion reservoir computing by utilizing the strain-induced nonlinear breathing dynamics of skyrmions [241]. Rajib et al. has found that the single-skyrmion system may have the highest performance while the capacities of the short-term memory and parity check in a multiple-skyrmion system are reduced due to the presence of spin-wave and dipolar interactions that may displace and distort skyrmions. Yokouchi et al. has experimentally constructed a skyrmion reservoir computing device by using the magnetic-field-induced dynamics of skyrmions [242]. This device consists of less than ten simply shaped, microscale Hall bars. In each Hall bar, skyrmions respond to the instantaneous input magnetic field pulse as well as to the memory of past field pulses. Input data are transformed into magnetic field pulse patterns with either square or sinusoidal shapes. The device has been verified to be successful in waveform recognition as well as in handwritten digital recognition with an accuracy of 94.7 %.

Other nonlinear dynamics of skyrmions have also been proposed for reservoir computing. Jiang et al. has studied through simulations a skyrmion reservoir by utilizing the skyrmion motion in a laterally asymmetric nanotrack [237]. The skyrmion position responds nonlinearly to input current pulses and acts as an output for image classification. Raab et al. has experimentally explored a skyrmion reservoir where a single skyrmion exists in a confined geometry of an equilateral triangle [182]. Voltages applied to the contacts at the three corners of the triangle control the skyrmion position due to the combined effects of the SOT, edge potential, and thermal fluctuations. From this, different Boolean operations of the device including AND, NAND, OR, NOR, XOR, and XNOR have been examined. Lee et al. has numerically investigated interactions of skyrmions with spin waves and has proposed a skyrmion spin-wave reservoir [238] that exploits spin waves propagating in a skyrmion crystal. The magnetization dynamics at the output end of the reservoir act as the output for classification and recognition tasks. Wang et al. has proposed a network of dynamic skyrmions for reservoir computing in which each skyrmion fluctuates in time between a small-skyrmion and large-skyrmion configuration, thereby behaving as a stochastic neuron [76]. Wang et al. has studied the dynamic interactions between neighboring skyrmions as well as the dynamic coupling strength which is a function of their separation distance and may serve as the node weight. The main challenges in implementing skyrmion reservoir computing are in regard to the optimization of skyrmion

reservoir conditions for applications and the integration of the skyrmion reservoir with other skyrmion synapse and neuron devices for signal readout and processing.

4. Conclusion

The failure of current CMOS-based computer paradigms in meeting the increasing demands of modern-day computation necessitates the development of post-von Neumann computing architectures. Spintronics represents an emerging class of technologies that takes advantage of the electron spin in conjunction with its charge. Recently, magnetic skyrmions have received notable attention as potential information carriers given their remarkable properties including nanoscale size, topological stability, effective controllability, high operational speed, low power consumption, and CMOS compatibility. The pursued goal of skyrmion-based electronics is to address the quickly approaching climax of von Neumann computing by the successful realization of these highly desirable properties.

Recent studies with either square or sinusoidal shapes the energy-efficient operation of global skyrmion motion through external magnetic [70,86–89] and electric [110–114] fields, charge/spin currents [71–74,76], thermal effects [90–93], as well as local defects [76,205,207]. The utilization of skyrmion motion has been put forward in racetrack memory [169] and logic devices [176–183], however the widespread implementation of these proposed systems is pending due to the difficulties in the reliable manipulation of skyrmion motion imposed by pinning effects, edge roughness, and the skyrmion Hall effect. Mechanisms to mitigate this detrimental effect include engineering geometric boundaries, local defects, and utilizing alternative magnetic textures such as skyrmioniums [156–158] and antiferromagnetic skyrmions [158–163]. Other magnetic textures such as skyrmion bundles [164,165] and bimerons [296–298] may also be applied in memory and logic devices. Particularly, the bimeron is a combination of a meron and an antimeron and is a skyrmion in in-plane magnetized magnets. Additionally, alternate three-dimensional magnetic structures such as chiral bobbers [174,175], skyrmion tubes, and hopfions [299] may also be realized by fabricating magnetic multilayers that possess both intralayer and interlayer DMIs. The newly identified interlayer DMI can govern a chiral magnetization across magnetic multilayers [300–303].

In addition to the memory and logic devices, skyrmions are also of interest to multiple unconventional computing devices [304]. Compared to the artificial neurons and synapses of CMOS-based ANNs, skyrmion-based counterparts have a lower spatial cost and consume much less energy with higher spatiotemporal stability. In the LIF model, the membrane potential is increased incrementally to a certain threshold under a series of input current pulses followed by an output spike and a reset of the membrane potential. For skyrmion neurons, the membrane potential can be marked by the skyrmion position in the nanotrack [222,226] or by other parameters such as the number of skyrmions pinned by the magnetic anisotropy barrier [220], the skyrmion size adjusted by the voltage-controlled PMA and strain [219,227], and the radius of the skyrmion motion in a skyrmion-based STNO [228]. The spike transmission process relies heavily on synaptic plasticity which is responsible for the modulation of synaptic weights and is determined either by the number of skyrmions or the skyrmion size. The potentiation and depression behaviors of a skyrmion synapse are modeled by the accumulation and dissipation of skyrmions which can be controlled by electrical currents [231,232,234], surface acoustic waves [230] and ultrafast laser pulses [233]. Research efforts have focused on achieving a compromise between the synaptic weight resolution, processing speed, functional area, and energy consumption by optimizing the track geometry and barrier design. Accomplishing successful operation of the skyrmion synapse at room temperature has attracted significant attention. Periodic multilayers have been proposed to reduce the fluctuations in skyrmion shape at room temperature [231]. By simulating a two-layer unsupervised ANN and a supervised deep ANN, the accuracy in pattern

recognition, optimization, and classification tasks at room temperature has been increased tremendously, indicating that skyrmion synapses are promising candidates for high-performance neuromorphic computing applications. The viable integration of skyrmion neurons and synapses, however, remains unresolved.

Skyrmion Brownian motion is an inherent random process that is invaluable to stochastic computing. Skyrmion-based TRNGs may be designed using a random distribution of skyrmions [191], the relative positions of two neighboring skyrmions [195], or the size fluctuation of an isolated skyrmion [76]. The resulting true random numbers are crucial for subsequent logic operations [91,92,243]. The high mobility, reversible polarity, and mutual interactions of skyrmions make them an ideal candidate for constructing efficient networks to solve optimization problems such as probabilistic inference, sampling, invertible logic, and integer factorization.

Reservoir computing for temporal information processing may utilize naturally-existing networks since the reservoirs do not require training. Magnetic skyrmions are suitable for realizing reservoir computing due to the emergence of organized skyrmion lattices along with their nonlinear response to external stimuli. Nonlinear dynamics of skyrmions include nonlinear current–voltage characteristics arising from skyrmion distortion [205,235,240,242] and geometric confinement [182] as well as from the strain-induced nonlinear breathing modes [241]. The outstanding obstacles to realizing skyrmion reservoir computing in practice include thermal fluctuations, low magnetoresistive signal, the pending optimization of skyrmion reservoir conditions, and the lack of integration of the skyrmion reservoir with other skyrmion synapse and neuron devices for signal readout and processing.

As with all spintronic applications, the creation and deletion of skyrmions, spatial cost, thermal stability, operation speed, and manufacturability are crucial parameters.

Generally, skyrmions can be nucleated from topologically trivial bubbles which can then relax into skyrmions or be transformed from stripe domains under a spin current [150]. Annihilation of a skyrmion is achieved by driving it to a boundary or by exerting a localized spin torque to transform it into the ferromagnetic state [150]. Recent studies have relaxed the conditions on the creation and stabilization of skyrmions from cryogenic, finite-field to room-temperature, magnetic field-free [70]. The challenge remains as to how to generate and stabilize a single skyrmion deterministically.

The skyrmion configuration is determined by the competition between multiple energy terms. Engineering material parameters to yield smaller skyrmions is crucial to addressing the issue of spatial cost in device applications. In addition to exploring new material systems to tune the intrinsic magnetic parameters [58], external controls including the voltage, strain, and chemisorption/desorption may also be used [110–117]. The magneto-ionic functionality has been proposed for modeling low-power-consumption, non-volatile memory devices [110] as well as artificial neurons [227] and synapses [266,267] based on multistate skyrmions.

Skyrmion stability is also of great significance to device applications. This can be achieved by striking a balance between the thermal forces that act on a skyrmion and the pinning effects inherent to the sample. Although strong pinning centers tend to impede skyrmion motion, pinning centers with intermediate strengths can be used to stabilize skyrmions and guide them in a predictable manner [118]. While elevated temperatures reduce the stability of these topological defects, they can also improve skyrmion mobility. Hence, a balance must be maintained between pinning center distribution and thermal effects to increase the lifetime of skyrmions in magnetic systems. The spatial inhomogeneity of magnetic parameters also plays a significant role by exerting pinning effects which induce local dynamics of skyrmions for versatile applications such as the non-linear response of the resistance [205], adder/subtractor operations [207], and TRNG [76]. The energy profiles of pinning, however, are rarely investigated and require further research to better understand the energy landscape. Fundamental

questions remain as to what types of energy profiles can be induced by different kinds of pinning and how to balance the effective manipulation of skyrmions with their thermal stability.

Another important parameter of spintronic devices is operation speed. High speeds can be achieved by reducing both the number and strength of pinning centers in the sample as well as by increasing the magnitude of the stimulus force. The theorized finite inertial mass of a skyrmion also suggests that reducing its size can help increase its speed.

Finally, most of the skyrmionic applications remain in the stage of conceptualization and prototyping. Careful consideration should be given to overcoming these current limitations in order to manufacture reliably robust and scalable skyrmionic devices that are competitive for next-generation technologies.

CRediT authorship contribution statement

Kang Wang: Conceptualization, Investigation, Writing – original draft, Writing – review & editing, Visualization. **Vineetha Bheemarasetty:** Investigation, Writing – original draft. **Junhang Duan:** Investigation, Writing – original draft. **Shiyu Zhou:** Investigation, Writing – original draft. **Gang Xiao:** Writing – review & editing, Funding acquisition.

Declaration of Competing Interest

The authors declare that they have no known competing financial interests or personal relationships that could have appeared to influence the work reported in this paper.

Data availability

Data will be made available on request.

Acknowledgements

References

[1] G.E. Moore, No exponential is forever: but" Forever" can be delayed! [semiconductor industry], in: 2003 IEEE International Solid-State Circuits Conference, 2003. Digest of Technical Papers. ISSCC., IEEE, 2003, pp. 20-23.

[2] R.G. Dreslinski, M. Wieckowski, D. Blaauw, D. Sylvester, T. Mudge, Near-threshold computing: Reclaiming moore's law through energy efficient integrated circuits, Proc. IEEE 98 (2010) 253–266.

[3] S. Petrenko, Limitations of von neumann architecture, in: Big Data Technologies for Monitoring of Computer Security: A Case Study of the Russian Federation, Springer, 2018, pp. 115-173.

[4] H.E. Yantır, A.M. Eltawil, K.N. Salama, A hardware/software co-design methodology for in-memory processors, J. Parallel Distrib. Comput. 161 (2022) 63–71.

[5] A.C. Sodan, J. Machina, A. Deshmeh, K. Macnaughton, B. Esbaugh, Parallelism via multithreaded and multicore CPUs, Computer 43 (2010) 24–32.

[6] P. Barla, V.K. Joshi, S. Bhat, Spintronic devices: a promising alternative to CMOS devices, J. Comput. Electron. 20 (2021) 805–837.

[7] A. Makarov, T. Windbacher, V. Sverdlov, S. Selberherr, CMOS-compatible spintronic devices: a review, Semicond. Sci. Technol. 31 (2016), 113006.

[8] G. Finocchio, M. Di Ventra, K.Y. Camsari, K. Everschor-Sitte, P.K. Amiri, Z. Zeng, The promise of spintronics for unconventional computing, J. Magn. Magn. Mater. 521 (2021), 167506.

[9] J. Zhou, J. Chen, Prospect of Spintronics in Neuromorphic Computing, Adv. Electron. Mater. 7 (2021) 2100465.

[10] J. Grollier, D. Querlioz, K. Camsari, K. Everschor-Sitte, S. Fukami, M.D. Stiles, Neuromorphic spintronics, Nat. Electron. 3 (2020) 360–370.

[11] T. Blachowicz, A. Ehrmann, Magnetic elements for neuromorphic computing, Molecules 25 (2020) 2550.

[12] A. Fert, N. Reyren, V. Cros, Magnetic skyrmions: advances in physics and potential applications, Nat. Rev. Mater. 2 (2017) 17031.

[13] A. Soumyanarayanan, N. Reyren, A. Fert, C. Panagopoulos, Emergent phenomena induced by spin–orbit coupling at surfaces and interfaces, Nature 539 (2016) 509–517.

[14] C. Back, V. Cros, H. Ebert, K. Everschor-Sitte, A. Fert, M. Garst, T. Ma, S. Mankovsky, T. Monchesky, M. Mostovoy, The 2020 skyrmionics roadmap, J. Phys. D: Appl. Phys. 53 (2020), 363001.

[15] M. Julliere, Tunneling between ferromagnetic films, Phys. Lett. A 54 (1975) 225–226.

[16] T. Miyazaki, N. Tezuka, Giant magnetic tunneling effect in Fe/Al2O3/Fe junction, J. Magn. Magn. Mater. 139 (1995) L231–L234.

[17] J.S. Moodera, L.R. Kinder, T.M. Wong, R. Meservey, Large magnetoresistance at room temperature in ferromagnetic thin film tunnel junctions, Phys. Rev. Lett. 74 (1995) 3273.

[18] W. Butler, X.-G. Zhang, T. Schulthess, J. MacLaren, Spin-dependent tunneling conductance of Fe| MgO| Fe sandwiches, Phys. Rev. B 63 (2001), 054416.

[19] J. Mathon, A. Umerski, Theory of tunneling magnetoresistance of an epitaxial Fe/ MgO/Fe (001) junction, Phys. Rev. B 63 (2001), 220403.

[20] M. Bowen, V. Cros, F. Petroff, A. Fert, C. Martinez Boubeta, J.L. Costa-Krämer, J. V. Anguita, A. Cebollada, F. Briones, J. De Teresa, Large magnetoresistance in Fe/ MgO/FeCo (001) epitaxial tunnel junctions on GaAs (001), Appl. Phys, Lett. 79 (2001) 1655–1657.

[21] S. Yuasa, T. Nagahama, A. Fukushima, Y. Suzuki, K. Ando, Giant room-temperature magnetoresistance in single-crystal Fe/MgO/Fe magnetic tunnel junctions, Nat. Mater. 3 (2004) 868–871.

[22] S.S. Parkin, C. Kaiser, A. Panchula, P.M. Rice, B. Hughes, M. Samant, S.-H. Yang, Giant tunnelling magnetoresistance at room temperature with MgO (100) tunnel barriers, Nat. Mater. 3 (2004) 862–867.

[23] S. Ikeda, J. Hayakawa, Y. Ashizawa, Y. Lee, K. Miura, H. Hasegawa, M. Tsunoda, F. Matsukura, H. Ohno, Tunnel magnetoresistance of 604% at 300 K by suppression of Ta diffusion in Co Fe B/ Mg O/ Co Fe B pseudo-spin-valves annealed at high temperature, Appl. Phys, Lett. 93 (2008) 082508.

[24] W. Egelhoff Jr, V. Höink, J. Lau, W. Shen, B. Schrag, G. Xiao, Magnetic tunnel junctions with large tunneling magnetoresistance and small saturation fields, J. Appl. Phys. 107 (2010) 09C705.

[25] J.C. Sankey, Y.-T. Cui, J.Z. Sun, J.C. Slonczewski, R.A. Buhrman, D.C. Ralph, Measurement of the spin-transfer-torque vector in magnetic tunnel junctions, Nat. Phys. 4 (2008) 67–71.

[26] Z. Diao, Z. Li, S. Wang, Y. Ding, A. Panchula, E. Chen, L.-C. Wang, Y. Huai, Spin-transfer torque switching in magnetic tunnel junctions and spin-transfer torque random access memory, J. Condens. Matter. Phys. 19 (2007), 165209.

[27] J. Sun, D. Ralph, Magnetoresistance and spin-transfer torque in magnetic tunnel junctions, J. Magn. Magn. Mater. 320 (2008) 1227–1237.

[28] M. Cubukcu, O. Boulle, M. Drouard, K. Garello, C. Onur Avci, I. Mihai Miron, J. Langer, B. Ocker, P. Gambardella, G. Gaudin, Spin-orbit torque magnetization switching of a three-terminal perpendicular magnetic tunnel junction, Appl. Phys, Lett., 104 (2014) 042406.

[29] E. Grimaldi, V. Krizakova, G. Sala, F. Yasin, S. Couet, G. Sankar Kar, K. Garello, P. Gambardella, Single-shot dynamics of spin–orbit torque and spin transfer torque switching in three-terminal magnetic tunnel junctions, Nat. Nanotechnol. 15 (2020) 111–117.

[30] W. Kong, C. Wan, C. Guo, C. Fang, B. Tao, X. Wang, X. Han, All-electrical manipulation of magnetization in magnetic tunnel junction via spin–orbit torque, Appl. Phys, Lett. 116 (2020), 162401.

[31] W.J. Gallagher, S.S. Parkin, Development of the magnetic tunnel junction MRAM at IBM: From first junctions to a 16-Mb MRAM demonstrator chip, IBM J. Res. Dev. 50 (2006) 5–23.

[32] H. Yoda, T. Kishi, T. Nagase, M. Yoshikawa, K. Nishiyama, E. Kitagawa, T. Daibou, M. Amano, N. Shimomura, S. Takahashi, High efficient spin transfer torque writing on perpendicular magnetic tunnel junctions for high density MRAMs, Curr. Appl. Phys. 10 (2010) e87–e89.

[33] W. Gallagher, E. Chien, T.-W. Chiang, J.-C. Huang, M.-C. Shih, C. Wang, C.-H. Weng, S. Chen, C. Bair, G. Lee, 22nm STT-MRAM for reflow and automotive uses with high yield, reliability, and magnetic immunity and with performance and shielding options, in: 2019 IEEE International Electron Devices Meeting (IEDM), IEEE, 2019, pp. 2.7. 1-2.7. 4.

[34] J. Alzate, U. Arslan, P. Bai, J. Brockman, Y.-J. Chen, N. Das, K. Fischer, T. Ghani, P. Heil, P. Hentges, 2 MB array-level demonstration of STT-MRAM process and performance towards L4 cache applications, in: 2019 IEEE International Electron Devices Meeting (IEDM), IEEE, 2019, pp. 2.4. 1-2.4. 4.

[35] V. Naik, K. Lee, K. Yamane, R. Chao, J. Kwon, N. Thiyagarajah, N. Chung, S. Jang, B. Behin-Aein, J. Lim, Manufacturable 22nm FD-SOI embedded MRAM technology for industrial-grade MCU and IOT applications, in: 2019 IEEE International Electron Devices Meeting (IEDM), IEEE, 2019, pp. 2.3. 1-2.3. 4.

[36] Y. Song, J. Lee, S. Han, H. Shin, K. Lee, K. Suh, D. Jeong, G. Koh, S. Oh, J. Park, Demonstration of highly manufacturable STT-MRAM embedded in 28nm logic, in: 2018 IEEE International Electron Devices Meeting (IEDM), IEEE, 2018, pp. 18.12. 11-18.12. 14.

[37] G. He, Y. Zhang, Y. Hu, X. Zhang, G. Xiao, Magnetic tunnel junction based gradiometer for detection of cracks in cement, Sens. Actuator A: Phys. 331 (2021), 112966.

[38] G. He, Y. Zhang, G. Xiao, Nonhysteretic Vortex Magnetic Tunnel Junction Sensor with High Dynamic Reserve, Phys. Rev. Appl. 14 (2020), 034051.

[39] Y. Zhang, G. He, X. Zhang, G. Xiao, Magnetotransport and electronic noise in superparamagnetic magnetic tunnel junctions, Appl. Phys, Lett. 115 (2019), 022402.

[40] W. Zhang, Q. Hao, G. Xiao, Low-frequency noise in serial arrays of MgO-based magnetic tunnel junctions, Phys. Rev. B 84 (2011), 094446.

[41] W. Zhang, G. Xiao, M.J. Carter, Two-dimensional field-sensing map and magnetic anisotropy dispersion in magnetic tunnel junction arrays, Phys. Rev. B 83 (2011), 144416.

[42] E. Paz, S. Serrano-Guisan, R. Ferreira, P. Freitas, Room temperature direct detection of low frequency magnetic fields in the 100 pT/Hz0. 5 range using large arrays of magnetic tunnel junctions, J. Appl. Phys., 115 (2014) 17E501.

[43] S. Cardoso, D. Leitao, L. Gameiro, F. Cardoso, R. Ferreira, E. Paz, P. Freitas, Magnetic tunnel junction sensors with pTesla sensitivity, Microsyst. Technol. 20 (2014) 793–802.

[44] R. Guerrero, M. Pannetier-Lecoeur, C. Fermon, S. Cardoso, R. Ferreira, P. Freitas, Low frequency noise in arrays of magnetic tunnel junctions connected in series and parallel, J. Appl. Phys. 105 (2009) 113922.

[45] K.Y. Camsari, R. Faria, B.M. Sutton, S. Datta, Stochastic p-bits for invertible logic, Phys. Rev. X 7 (2017), 031014.

[46] K. Hayakawa, S. Kanai, T. Funatsu, J. Igarashi, B. Jinnai, W. Borders, H. Ohno, S. Fukami, Nanosecond random telegraph noise in in-plane magnetic tunnel junctions, Phys. Rev. Lett. 126 (2021), 117202.

[47] C. Safranski, J. Kaiser, P. Trouilloud, P. Hashemi, G. Hu, J.Z. Sun, Demonstration of nanosecond operation in stochastic magnetic tunnel junctions, Nano Lett. 21 (2021) 2040–2045.

[48] J. Kaiser, W.A. Borders, K.Y. Camsari, S. Fukami, H. Ohno, S. Datta, Hardware-Aware In Situ Learning Based on Stochastic Magnetic Tunnel Junctions, Phys. Rev. Appl. 17 (2022), 014016.

[49] W.A. Borders, A.Z. Pervaiz, S. Fukami, K.Y. Camsari, H. Ohno, S. Datta, Integer factorization using stochastic magnetic tunnel junctions, Nature 573 (2019) 390–393.

[50] M. Romera, P. Talatchian, S. Tsunegi, F. Abreu Araujo, V. Cros, P. Bortolotti, J. Trastoy, K. Yakushiji, A. Fukushima, H. Kubota, Vowel recognition with four coupled spin-torque nano-oscillators, Nature 563 (2018) 230–234.

[51] M. Tarequzzaman, T. Böhnert, M. Decker, J. Costa, J. Borme, B. Lacoste, E. Paz, A. Jenkins, S. Serrano-Guisan, C. Back, Spin torque nano-oscillator driven by combined spin injection from tunneling and spin Hall current, Commun. Phys. 2 (2019) 1–8.

[52] M. Zahedinejad, A.A. Awad, S. Muralidhar, R. Khymyn, H. Fulara, H. Mazraati, M. Dvornik, J. Åkerman, Two-dimensional mutually synchronized spin Hall nano-oscillator arrays for neuromorphic computing, Nat. Nanotechnol. 15 (2020) 47–52.

[53] R.V. Ababei, M.O. Ellis, I.T. Vidamour, D.S. Devadasan, D.A. Allwood, E. Vasilaki, T.J. Hayward, Neuromorphic computation with a single magnetic domain wall, Sci. Rep. 11 (2021) 1–13.

[54] D. Kumar, T. Jin, R. Sbiaa, M. Kläui, S. Bedanta, S. Fukami, D. Ravelosona, S.-H. Yang, X. Liu, S. Piramanayagam, Domain wall memory: Physics, materials, and devices, Phys. Rep. 958 (2022) 1–35.

[55] S. Liu, C.H. Bennett, J.S. Friedman, M.J. Marinella, D. Paydarfar, J.A.C. Incorvia, Controllable reset behavior in domain wall–magnetic tunnel junction artificial neurons for task-adaptable computation, IEEE Magn. Lett. 12 (2021) 1–5.

[56] W.H. Brigner, N. Hassan, L. Jiang-Wei, X. Hu, D. Saha, C.H. Bennett, M. J. Marinella, J.A.C. Incorvia, F. Garcia-Sanchez, J.S. Friedman, Shape-based magnetic domain wall drift for an artificial spintronic leaky integrate-and-fire neuron, IEEE Trans. Electron Devices 66 (2019) 4970–4975.

[57] A. Sengupta, K. Roy, Encoding neural and synaptic functionalities in electron spin: A pathway to efficient neuromorphic computing, Appl. Phys. Rev. 4 (2017), 041105.

[58] Y. Tokura, N. Kanazawa, Magnetic skyrmion materials, Chem. Rev. 121 (2020) 2857–2897.

[59] K. Everschor-Sitte, J. Masell, R.M. Reeve, M. Kläui, Perspective: Magnetic skyrmions—Overview of recent progress in an active research field, J. Appl. Phys. 124 (2018), 240901.

[60] K. Karube, J.S. White, D. Morikawa, C.D. Dewhurst, R. Cubitt, A. Kikkawa, X. Yu, Y. Tokunaga, T.-h. Arima, H.M. Rønnow, Disordered skyrmion phase stabilized by magnetic frustration in a chiral magnet, Sci. Adv., 4 (2018) eaar7043.

[61] A. Chacon, L. Heinen, M. Halder, A. Bauer, W. Simeth, S. Mühlbauer, H. Berger, M. Garst, A. Rosch, C. Pfleiderer, Observation of two independent skyrmion phases in a chiral magnetic material, Nat. Phys. 14 (2018) 936–941.

[62] A.K. Nayak, V. Kumar, T. Ma, P. Werner, E. Pippel, R. Sahoo, F. Damay, U. K. Rößler, C. Felser, S.S. Parkin, Magnetic antiskyrmions above room temperature in tetragonal Heusler materials, Nature 548 (2017) 561–566.

[63] I. Kézsmárki, S. Bordács, P. Milde, E. Neuber, L. Eng, J. White, H.M. Rønnow, C. Dewhurst, M. Mochizuki, K. Yanai, Néel-type skyrmion lattice with confined orientation in the polar magnetic semiconductor GaV4S8, Nat. Mater. 14 (2015) 1116–1122.

[64] K. Karube, J.S. White, D. Morikawa, M. Bartkowiak, A. Kikkawa, Y. Tokunaga, T. Arima, H.M. Rønnow, Y. Tokura, Y. Taguchi, Skyrmion formation in a bulk chiral magnet at zero magnetic field and above room temperature, Phys. Rev. Mater. 1 (2017), 074405.

[65] S. Seki, X. Yu, S. Ishiwata, Y. Tokura, Observation of skyrmions in a multiferroic material, Science 336 (2012) 198–201.

[66] X. Yu, Y. Onose, N. Kanazawa, J.H. Park, J. Han, Y. Matsui, N. Nagaosa, Y. Tokura, Real-space observation of a two-dimensional skyrmion crystal, Nature 465 (2010) 901–904.

[67] S. Mühlbauer, B. Binz, F. Jonietz, C. Pfleiderer, A. Rosch, A. Neubauer, R. Georgii, P. Böni, Skyrmion lattice in a chiral magnet, Science 323 (2009) 915–919.

[68] X. Yu, N. Kanazawa, Y. Onose, K. Kimoto, W. Zhang, S. Ishiwata, Y. Matsui, Y. Tokura, Near room-temperature formation of a skyrmion crystal in thin-films of the helimagnet FeGe, Nat. Mater. 10 (2011) 106–109.

[69] K. Shibata, X. Yu, T. Hara, D. Morikawa, N. Kanazawa, K. Kimoto, S. Ishiwata, Y. Matsui, Y. Tokura, Towards control of the size and helicity of skyrmions in helimagnetic alloys by spin–orbit coupling, Nat. Nanotechnol. 8 (2013) 723–728.

[70] F. Büttner, I. Lemesh, M. Schneider, B. Pfau, C.M. Günther, P. Hessing, J. Geilhufe, L. Caretta, D. Engel, B. Krüger, Field-free deterministic ultrafast creation of magnetic skyrmions by spin–orbit torques, Nat. Nanotechnol. 12 (2017) 1040–1044.

[71] K. Litzius, I. Lemesh, B. Krüger, P. Bassirian, L. Caretta, K. Richter, F. Büttner, K. Sato, O.A. Tretiakov, J. Förster, Skyrmion Hall effect revealed by direct time-resolved X-ray microscopy, Nat. Phys. 13 (2017) 170–175.

[72] W. Jiang, X. Zhang, G. Yu, W. Zhang, X. Wang, M. Benjamin Jungfleisch, J. E. Pearson, X. Cheng, O. Heinonen, K.L. Wang, Direct observation of the skyrmion Hall effect, Nat. Phys. 13 (2017) 162–169.

[73] S. Woo, K. Litzius, B. Krüger, M.-Y. Im, L. Caretta, K. Richter, M. Mann, A. Krone, R.M. Reeve, M. Weigand, Observation of room-temperature magnetic skyrmions and their current-driven dynamics in ultrathin metallic ferromagnets, Nat. Mater. 15 (2016) 501–506.

[74] W. Jiang, P. Upadhyaya, W. Zhang, G. Yu, M.B. Jungfleisch, F.Y. Fradin, J. E. Pearson, Y. Tserkovnyak, K.L. Wang, O. Heinonen, Blowing magnetic skyrmion bubbles, Science 349 (2015) 283–286.

[75] K. Wang, L. Qian, W. Chen, S.-C. Ying, G. Xiao, X. Wu, Spin torque effect on topological defects and transitions of magnetic domain phases in Ta/CoFeB/MgO, Phys. Rev. B 99 (2019), 184410.

[76] K. Wang, Y. Zhang, V. Bheemarasetty, S. Zhou, S.-C. Ying, G. Xiao, Single skyrmion true random number generator using local dynamics and interaction between skyrmions, Nat. Commun. 13 (2022) 722.

[77] C. Moreau-Luchaire, C. Moutafis, N. Reyren, J. Sampaio, C. Vaz, N. Van Horne, K. Bouzehouane, K. Garcia, C. Deranlot, P. Warnicke, Additive interfacial chiral interaction in multilayers for stabilization of small individual skyrmions at room temperature, Nat. Nanotechnol. 11 (2016) 444–448.

[78] R. Ozawa, S. Hayami, Y. Motome, Zero-field skyrmions with a high topological number in itinerant magnets, Phys. Rev. Lett. 118 (2017), 147205.

[79] C.D. Batista, S.-Z. Lin, S. Hayami, Y. Kamiya, Frustration and chiral orderings in correlated electron systems, Rep. Prog. Phys. 79 (2016), 084504.

[80] A. Leonov, M. Mostovoy, Multiply periodic states and isolated skyrmions in an anisotropic frustrated magnet, Nat. Commun. 6 (2015) 8275.

[81] T. Okubo, S. Chung, H. Kawamura, Multiple-q states and the skyrmion lattice of the triangular-lattice Heisenberg antiferromagnet under magnetic fields, Phys. Rev. Lett. 108 (2012), 017206.

[82] J. Iwasaki, M. Mochizuki, N. Nagaosa, Current-induced skyrmion dynamics in constricted geometries, Nat. Nanotechnol. 8 (2013) 742–747.

[83] H. Du, R. Che, L. Kong, X. Zhao, C. Jin, C. Wang, J. Yang, W. Ning, R. Li, C. Jin, Edge-mediated skyrmion chain and its collective dynamics in a confined geometry, Nat. Commun. 6 (2015) 8504.

[84] D.A. Gilbert, B.B. Maranville, A.L. Balk, B.J. Kirby, P. Fischer, D.T. Pierce, J. Unguris, J.A. Borchers, K. Liu, Realization of ground-state artificial skyrmion lattices at room temperature, Nat. Commun. 6 (2015) 8462.

[85] C. Song, N. Kerber, J. Rothörl, Y. Ge, K. Raab, B. Seng, M.A. Brems, F. Dittrich, R. M. Reeve, J. Wang, Commensurability between element symmetry and the number of skyrmions governing skyrmion diffusion in confined geometries, Adv. Funct. Mater. 31 (2021) 2010739.

[86] S. Zhang, W. Wang, D. Burn, H. Peng, H. Berger, A. Bauer, C. Pfleiderer, G. Van Der Laan, T. Hesjedal, Manipulation of skyrmion motion by magnetic field gradients, Nat. Commun. 9 (2018) 2115.

[87] S. Zhang, J. Zhang, Q. Zhang, C. Barton, V. Neu, Y. Zhao, Z. Hou, Y. Wen, C. Gong, O. Kazakova, Direct writing of room temperature and zero field skyrmion lattices by a scanning local magnetic field, Appl. Phys. Lett. 112 (2018), 132405.

[88] A. Casiraghi, H. Corte-León, M. Vafaee, F. Garcia-Sanchez, G. Durin, M. Pasquale, G. Jakob, M. Kläui, O. Kazakova, Individual skyrmion manipulation by local magnetic field gradients, Commun. Phys. 2 (2019) 1–9.

[89] K. Migita, K. Yamada, Y. Nakatani, Controlling skyrmion motion in an angelfish-type racetrack memory by an AC magnetic field, Appl. Phys. Express 13 (2020), 073003.

[90] M. Mochizuki, X. Yu, S. Seki, N. Kanazawa, W. Koshibae, J. Zang, M. Mostovoy, Y. Tokura, N. Nagaosa, Thermally driven ratchet motion of a skyrmion microcrystal and topological magnon Hall effect, Nat. Mater. 13 (2014) 241–246.

[91] D. Pinna, F.A. Araujo, J.-V. Kim, V. Cros, D. Querlioz, P. Bessière, J. Droulez, J. Grollier, Skyrmion gas manipulation for probabilistic computing, Phys. Rev. Appl. 9 (2018), 064018.

[92] J. Zázvorka, F. Jakobs, D. Heinze, N. Keil, S. Kromin, S. Jaiswal, K. Litzius, G. Jakob, P. Virnau, D. Pinna, Thermal skyrmion diffusion used in a reshuffler device, Nat. Nanotechnol. 14 (2019) 658–661.

[93] Z. Wang, M. Guo, H.-A. Zhou, L. Zhao, T. Xu, R. Tomasello, H. Bai, Y. Dong, S.-G. Je, W. Chao, Thermal generation, manipulation and thermoelectric detection of skyrmions, Nat. Electron. 3 (2020) 672–679.

[94] H. Yang, M. Chshiev, B. Dieny, J. Lee, A. Manchon, K. Shin, First-principles investigation of the very large perpendicular magnetic anisotropy at Fe| MgO and Co| MgO interfaces, Phys. Rev. B 84 (2011), 054401.

[95] B. Dieny, M. Chshiev, Perpendicular magnetic anisotropy at transition metal/ oxide interfaces and applications, Rev. Mod. Phys. 89 (2017), 025008.

[96] I. Dzyaloshinsky, A thermodynamic theory of "weak" ferromagnetism of antiferromagnetics, J. Phys. Chem. Solids 4 (1958) 241–255.

[97] T. Moriya, Anisotropic superexchange interaction and weak ferromagnetism, Phys. Rev. 120 (1960) 91.

[98] H. Yang, A. Thiaville, S. Rohart, A. Fert, M. Chshiev, Anatomy of dzyaloshinskii-moriya interaction at Co/Pt interfaces, Phys. Rev. Lett. 115 (2015), 267210.

[99] J. Iwasaki, M. Mochizuki, N. Nagaosa, Universal current-velocity relation of skyrmion motion in chiral magnets, Nat. Commun. 4 (2013) 1463.

[100] J.H. Han, J. Zang, Z. Yang, J.-H. Park, N. Nagaosa, Skyrmion lattice in a two-dimensional chiral magnet, Phys. Rev. B 82 (2010) 094429.

[101] J. Rowland, S. Banerjee, M. Randeria, Skyrmions in chiral magnets with Rashba and Dresselhaus spin-orbit coupling, Phys. Rev. B 93 (2016), 020404.

[102] H. Wu, X. Hu, K. Jing, X. Wang, Size and profile of skyrmions in skyrmion crystals, Commun. Phys. 4 (2021) 1–7.

[103] N. Romming, C. Hanneken, M. Menzel, J.E. Bickel, B. Wolter, K. von Bergmann, A. Kubetzka, R. Wiesendanger, Writing and deleting single magnetic skyrmions, Science 341 (2013) 636–639.

[104] N. Romming, A. Kubetzka, C. Hanneken, K. von Bergmann, R. Wiesendanger, Field-dependent size and shape of single magnetic skyrmions, Phys. Rev. Lett. 114 (2015), 177203.

[105] S. Jaiswal, K. Litzius, I. Lemesh, F. Büttner, S. Finizio, J. Raabe, M. Weigand, K. Lee, J. Langer, B. Ocker, Investigation of the Dzyaloshinskii-Moriya interaction and room temperature skyrmions in W/CoFeB/MgO thin films and microwires, Appl. Phys. Lett. 111 (2017), 022409.

[106] G. Yu, P. Upadhyaya, X. Li, W. Li, S.K. Kim, Y. Fan, K.L. Wong, Y. Tserkovnyak, P. K. Amiri, K.L. Wang, Room-temperature creation and spin–orbit torque manipulation of skyrmions in thin films with engineered asymmetry, Nano Lett. 16 (2016) 1981–1988.

[107] T. Meier, M. Kronseder, C. Back, Domain-width model for perpendicularly magnetized systems with Dzyaloshinskii-Moriya interaction, Phys. Rev. B 96 (2017), 144408.

[108] X. Wang, H. Yuan, X. Wang, A theory on skyrmion size, Commun. Phys. 1 (2018) 1–7.

[109] S. Rohart, A. Thiaville, Skyrmion confinement in ultrathin film nanostructures in the presence of Dzyaloshinskii-Moriya interaction, Phys. Rev. B 88 (2013), 184422.

[110] Y. Wang, L. Wang, J. Xia, Z. Lai, G. Tian, X. Zhang, Z. Hou, X. Gao, W. Mi, C. Feng, Electric-field-driven non-volatile multi-state switching of individual skyrmions in a multiferroic heterostructure, Nat. Commun. 11 (2020) 3577.

[111] D. Bhattacharya, S.A. Razavi, H. Wu, B. Dai, K.L. Wang, J. Atulasimha, Creation and annihilation of non-volatile fixed magnetic skyrmions using voltage control of magnetic anisotropy, Nat. Electron. 3 (2020) 539–545.

[112] H. Xia, C. Song, C. Jin, J. Wang, J. Wang, Q. Liu, Skyrmion motion driven by the gradient of voltage-controlled magnetic anisotropy, J. Magn. Magn. Mater. 458 (2018) 57–61.

[113] L. Zhao, X. Liang, J. Xia, G. Zhao, Y. Zhou, A ferromagnetic skyrmion-based diode with a voltage-controlled potential barrier, Nanoscale 12 (2020) 9507–9516.

[114] W. Kang, Y. Huang, C. Zheng, W. Lv, N. Lei, Y. Zhang, X. Zhang, Y. Zhou, W. Zhao, Voltage controlled magnetic skyrmion motion for racetrack memory, Sci. Rep. 6 (2016) 1–11.

[115] G. Chen, C. Ophus, A. Quintana, H. Kwon, C. Won, H. Ding, Y. Wu, A.K. Schmid, K. Liu, Reversible writing/deleting of magnetic skyrmions through hydrogen adsorption/desorption, Nat. Commun. 13 (2022) 1350.

[116] G. Chen, M. Robertson, M. Hoffmann, C. Ophus, A.L.F. Cauduro, R.L. Conte, H. Ding, R. Wiesendanger, S. Blügel, A.K. Schmid, Observation of hydrogen-induced Dzyaloshinskii-Moriya interaction and reversible switching of magnetic chirality, Phys. Rev. X 11 (2021), 021015.

[117] G. Chen, A. Mascaraque, H. Jia, B. Zimmermann, M. Robertson, R.L. Conte, M. Hoffmann, M.A. González Barrio, H. Ding, R. Wiesendanger, Large Dzyaloshinskii-Moriya interaction induced by chemisorbed oxygen on a ferromagnet surface, Sci. Adv., 6 (2020) eaba4924.

[118] C. Reichhardt, C. Reichhardt, M. Milosevic, Statics and dynamics of skyrmions interacting with pinning: a review, arXiv preprint arXiv:2102.10464, (2021).

[119] B. Cui, D. Yu, Z. Shao, Y. Liu, H. Wu, P. Nan, Z. Zhu, C. Wu, T. Guo, P. Chen, Néel-Type Elliptical Skyrmions in a Laterally Asymmetric Magnetic Multilayer, Adv. Mater. 33 (2021) 2006924.

[120] P. Huang, T. Schönenberger, M. Cantoni, L. Heinen, A. Magrez, A. Rosch, F. Carbone, H.M. Rønnow, Melting of a skyrmion lattice to a skyrmion liquid via a hexatic phase, Nat. Nanotechnol. 15 (2020) 761–767.

[121] J. Jena, B. Göbel, T. Ma, V. Kumar, R. Saha, I. Mertig, C. Felser, S.S. Parkin, Elliptical Bloch skyrmion chiral twins in an antiskyrmion system, Nat. Commun. 11 (2020) 1115.

[122] W. Legrand, D. Maccariello, N. Reyren, K. Garcia, C. Moutafis, C. Moreau-Luchaire, S. Collin, K. Bouzehouane, V. Cros, A. Fert, Room-temperature current-induced generation and motion of sub-100 nm skyrmions, Nano Lett. 17 (2017) 2703–2712.

[123] K. Ohara, X. Zhang, Y. Chen, Z. Wei, Y. Ma, J. Xia, Y. Zhou, X. Liu, Confinement and protection of skyrmions by patterns of modified magnetic properties, Nano Lett. 21 (2021) 4320–4326.

[124] C. Reichhardt, D. Ray, C.O. Reichhardt, Collective transport properties of driven skyrmions with random disorder, Phys. Rev. Lett. 114 (2015), 217202.

[125] I.L. Fernandes, J. Chico, S. Lounis, Impurity-dependent gyrotropic motion, deflection and pinning of current-driven ultrasmall skyrmions in PdFe/Ir (111) surface, J. Condens. Matter. Phys. 32 (2020), 425802.

[126] J. Castell-Queralt, L. González-Gómez, N. Del-Valle, A. Sanchez, C. Navau, Accelerating, guiding, and compressing skyrmions by defect rails, Nanoscale 11 (2019) 12589–12594.

[127] C. Reichhardt, D. Ray, C.O. Reichhardt, Quantized transport for a skyrmion moving on a two-dimensional periodic substrate, Phys. Rev. B 91 (2015), 104426.

[128] R. Gruber, J. Zázvorka, M.A. Brems, D.R. Rodrigues, T. Dohi, N. Kerber, B. Seng, K. Everschor-Sitte, P. Virnau, M. Kläui, Skyrmion pinning energetics in thin film systems, arXiv preprint arXiv:2201.01618, (2022).

[129] C. Reichhardt, D. Ray, C.O. Reichhardt, Magnus-induced ratchet effects for skyrmions interacting with asymmetric substrates, New J. Phys. 17 (2015), 073034.

[130] J. Feilhauer, S. Saha, J. Tobik, M. Zelent, L.J. Heyderman, M. Mruczkiewicz, Controlled motion of skyrmions in a magnetic antidot lattice, Phys. Rev. B 102 (2020), 184425.

[131] S. Zhang, Z. Li, Roles of nonequilibrium conduction electrons on the magnetization dynamics of ferromagnets, Phys. Rev. Lett. 93 (2004), 127204.

[132] E.I. Rashba, Properties of semiconductors with an extremum loop. I. Cyclotron and combinational resonance in a magnetic field perpendicular to the plane of the loop, Sov. Phys. Solid State 2 (1960) 1109–1122.

[133] L. Liu, O. Lee, T. Gudmundsen, D. Ralph, R. Buhrman, Current-induced switching of perpendicularly magnetized magnetic layers using spin torque from the spin Hall effect, Phys. Rev. Lett. 109 (2012), 096602.

[134] L. Liu, C.-F. Pai, Y. Li, H. Tseng, D. Ralph, R. Buhrman, Spin-torque switching with the giant spin Hall effect of tantalum, Science 336 (2012) 555–558.

[135] A. Hoffmann, Spin Hall effects in metals, IEEE Trans. Magn. 49 (2013) 5172–5193.

[136] Q. Hao, W. Chen, G. Xiao, Beta (β) tungsten thin films: Structure, electron transport, and giant spin Hall effect, Appl. Phys. Lett. 106 (2015), 182403.

[137] Q. Hao, G. Xiao, Giant spin Hall effect and switching induced by spin-transfer torque in a W/Co 40 Fe 40 B 20/MgO structure with perpendicular magnetic anisotropy, Phys. Rev. Appl. 3 (2015), 034009.

[138] J. Sinova, S.O. Valenzuela, J. Wunderlich, C. Back, T. Jungwirth, Spin hall effects, Rev. Mod. Phys. 87 (2015) 1213.

[139] W. Chen, L. Qian, G. Xiao, Deterministic current induced magnetic switching without external field using giant spin Hall effect of β-W, Sci. Rep. 8 (2018) 1–8.

[140] W. Chen, G. Xiao, Q. Zhang, X. Zhang, Temperature study of the giant spin Hall effect in the bulk limit of β− W, Phys. Rev. B 98 (2018), 134411.

[141] L. Qian, W. Chen, K. Wang, X. Wu, G. Xiao, Spin Hall effect and current induced magnetic switching in antiferromagnetic IrMn, AIP Adv. 8 (2018), 115323.

[142] L. Qian, K. Wang, Y. Zheng, G. Xiao, Spin Hall effect in the α and β phases of T a x W 1−x alloys, Phys. Rev. B 102 (2020), 094438.

[143] J.C. Slonczewski, Current-driven excitation of magnetic multilayers, J. Magn. Magn. Mater. 159 (1996) L1–L7.

[144] J. Xiao, A. Zangwill, M.D. Stiles, Boltzmann test of Slonczewski's theory of spin-transfer torque, Phys. Rev. B 70 (2004), 172405.

[145] K. Wang, L. Qian, S.-C. Ying, G. Xiao, X. Wu, Controlled modification of skyrmion information in a three-terminal racetrack memory, Nanoscale 11 (2019) 6952–6961.

[146] O. Heinonen, W. Jiang, H. Somaily, S.G. Te Velthuis, A. Hoffmann, Generation of magnetic skyrmion bubbles by inhomogeneous spin Hall currents, Phys. Rev. B 93 (2016), 094407.

[147] D. Maccariello, W. Legrand, N. Reyren, K. Garcia, K. Bouzehouane, S. Collin, V. Cros, A. Fert, Electrical detection of single magnetic skyrmions in metallic multilayers at room temperature, Nat. Nanotechnol. 13 (2018) 233–237.

[148] S. Woo, K.M. Song, X. Zhang, M. Ezawa, Y. Zhou, X. Liu, M. Weigand, S. Finizio, J. Raabe, M.-C. Park, Deterministic creation and deletion of a single magnetic skyrmion observed by direct time-resolved X-ray microscopy, Nat. Electron. 1 (2018) 288–296.

[149] J. Sampaio, V. Cros, S. Rohart, A. Thiaville, A. Fert, Nucleation, stability and current-induced motion of isolated magnetic skyrmions in nanostructures, Nat. Nanotechnol. 8 (2013) 839–844.

[150] X. Zhang, Y. Zhou, K.M. Song, T.-E. Park, J. Xia, M. Ezawa, X. Liu, W. Zhao, G. Zhao, S. Woo, Skyrmion-electronics: writing, deleting, reading and processing magnetic skyrmions toward spintronic applications, J. Condens. Matter. Phys. 32 (2020), 143001.

[151] S.-Z. Lin, Edge instability in a chiral stripe domain under an electric current and skyrmion generation, Phys. Rev. B 94 (2016), 020402.

[152] M. He, L. Peng, Z. Zhu, G. Li, J. Cai, J. Li, H. Wei, L. Gu, S. Wang, T. Zhao, Realization of zero-field skyrmions with high-density via electromagnetic manipulation in Pt/Co/Ta multilayers, Appl. Phys. Lett. 111 (2017), 202403.

[153] K. Litzius, J. Leliaert, P. Bassirian, D. Rodrigues, S. Kromin, I. Lemesh, J. Zazvorka, K.-J. Lee, J. Mulkers, N. Kerber, The role of temperature and drive current in skyrmion dynamics, Nat. Electron. 3 (2020) 30–36.

[154] A. Thiele, Steady-state motion of magnetic domains, Phys. Rev. Lett. 30 (1973) 230.

[155] S. Seki, M. Mochizuki, Skyrmions in magnetic materials, Springer, 2016.

[156] X. Zhang, J. Xia, Y. Zhou, D. Wang, X. Liu, W. Zhao, M. Ezawa, Control and manipulation of a magnetic skyrmionium in nanostructures, Phys. Rev. B 94 (2016), 094420.

[157] B. Göbel, A.F. Schäffer, J. Berakdar, I. Mertig, S.S. Parkin, Electrical writing, deleting, reading, and moving of magnetic skyrmioniums in a racetrack device, Sci. Rep. 9 (2019) 1–9.

[158] L. Shen, X. Li, Y. Zhao, J. Xia, G. Zhao, Y. Zhou, Current-induced dynamics of the antiferromagnetic skyrmion and skyrmionium, Phys. Rev. Appl. 12 (2019), 064033.

[159] J. Barker, O.A. Tretiakov, Static and dynamical properties of antiferromagnetic skyrmions in the presence of applied current and temperature, Phys. Rev. Lett. 116 (2016), 147203.

[160] C. Jin, C. Song, J. Wang, Q. Liu, Dynamics of antiferromagnetic skyrmion driven by the spin Hall effect, Appl. Phys. Lett. 109 (2016), 182404.

[161] X. Zhang, Y. Zhou, M. Ezawa, Antiferromagnetic skyrmion: stability, creation and manipulation, Sci. Rep. 6 (2016) 1–8.

[162] T. Dohi, S. DuttaGupta, S. Fukami, H. Ohno, Formation and current-induced motion of synthetic antiferromagnetic skyrmion bubbles, Nat. Commun. 10 (2019) 5153.

[163] W. Legrand, D. Maccariello, F. Ajejas, S. Collin, A. Vecchiola, K. Bouzehouane, N. Reyren, V. Cros, A. Fert, Room-temperature stabilization of antiferromagnetic skyrmions in synthetic antiferromagnets, Nat. Mater. 19 (2020) 34–42.

[164] J. Tang, Y. Wu, W. Wang, L. Kong, B. Lv, W. Wei, J. Zang, M. Tian, H. Du, Magnetic skyrmion bundles and their current-driven dynamics, Nat. Nanotechnol. 16 (2021) 1086–1091.

[165] W. Wang, D. Song, W. Wei, P. Nan, S. Zhang, B. Ge, M. Tian, J. Zang, H. Du, Electrical manipulation of skyrmions in a chiral magnet, Nat. Commun. 13 (2022) 1593.

[166] P. Lai, G. Zhao, H. Tang, N. Ran, S. Wu, J. Xia, X. Zhang, Y. Zhou, An improved racetrack structure for transporting a skyrmion, Sci. Rep. 7 (2017) 1–8.

[167] X. Zhang, G. Zhao, H. Fangohr, J.P. Liu, W. Xia, J. Xia, F. Morvan, Skyrmion-skyrmion and skyrmion-edge repulsions in skyrmion-based racetrack memory, Sci. Rep. 5 (2015) 1–6.

[168] I. Lima Fernandes, J. Bouaziz, S. Blügel, S. Lounis, Universality of defect-skyrmion interaction profiles, Nat. Commun. 9 (2018) 4395.

[169] A. Fert, V. Cros, J. Sampaio, Skyrmions on the track, Nat. Nanotechnol. 8 (2013) 152–156.

[170] S.S. Parkin, M. Hayashi, L. Thomas, Magnetic domain-wall racetrack memory, Science 320 (2008) 190–194.

[171] R. Tomasello, E. Martinez, R. Zivieri, L. Torres, M. Carpentieri, G. Finocchio, A strategy for the design of skyrmion racetrack memories, Sci. Rep. 4 (2014) 1–7.

[172] W. Kang, C. Zheng, Y. Huang, X. Zhang, Y. Zhou, W. Lv, W. Zhao, Complementary skyrmion racetrack memory with voltage manipulation, IEEE Electron Device Lett. 37 (2016) 924–927.

[173] D. Zhu, W. Kang, S. Li, Y. Huang, X. Zhang, Y. Zhou, W. Zhao, Skyrmion racetrack memory with random information update/deletion/insertion, IEEE Trans. Electron Devices 65 (2017) 87–95.

[174] J. Zhu, Y. Wu, Q. Hu, L. Kong, J. Tang, M. Tian, H. Du, Current-driven transformations of a skyrmion tube and a bobber in stepped nanostructures of chiral magnets, Sci. China: Phys. Mech. Astron. 64 (2021) 1–6.

[175] F. Zheng, F.N. Rybakov, A.B. Borisov, D. Song, S. Wang, Z.-A. Li, H. Du, N. S. Kiselev, J. Caron, A. Kovács, Experimental observation of chiral magnetic bobbers in B20-type FeGe, Nat. Nanotechnol. 13 (2018) 451–455.

[176] S. Luo, L. You, Skyrmion devices for memory and logic applications, APL Mater. 9 (2021), 050901.

[177] X. Zhang, M. Ezawa, Y. Zhou, Magnetic skyrmion logic gates: conversion, duplication and merging of skyrmions, Sci. Rep. 5 (2015) 1–8.

[178] X. Xing, P.W. Pong, Y. Zhou, Skyrmion domain wall collision and domain wall-gated skyrmion logic, Phys. Rev. B 94 (2016), 054408.

[179] Z. He, S. Angizi, D. Fan, Current-induced dynamics of multiple skyrmions with domain-wall pair and skyrmion-based majority gate design, IEEE Magn. Lett. 8 (2017) 1–5.

[180] S. Luo, M. Song, X. Li, Y. Zhang, J. Hong, X. Yang, X. Zou, N. Xu, L. You, Reconfigurable skyrmion logic gates, Nano Lett. 18 (2018) 1180–1184.

[181] Z. Yan, Y. Liu, Y. Guang, K. Yue, J. Feng, R. Lake, G. Yu, X. Han, Skyrmion-Based Programmable Logic Device with Complete Boolean Logic Functions, Phys. Rev. Appl. 15 (2021), 064004.

[182] K. Raab, M.A. Brems, G. Beneke, T. Dohi, J. Rothörl, J.H. Mentink, M. Kläui, Brownian reservoir computing realized using geometrically confined skyrmions, arXiv preprint arXiv:2203.14720, (2022).

[183] D. Yu, H. Yang, M. Chshiev, A. Fert, Skyrmions-based logic gates in one single nanotrack completely reconstructed via chirality barrie, arXiv preprint arXiv: 2201.06182, (2022).

[184] B. Paikaray, M. Kuchibhotla, A. Haldar, C. Murapaka, Reconfigurable Logic Operations via Gate Controlled Skyrmion Motion in a Nanomagnetic Device, ACS Appl, Electron. Mater. (2022).

[185] J. Miltat, S. Rohart, A. Thiaville, Brownian motion of magnetic domain walls and skyrmions, and their dependence on diffusion constants, Phys. Rev. B 97 (2018), 214426.

[186] T. Nozaki, Y. Jibiki, M. Goto, E. Tamura, T. Nozaki, H. Kubota, A. Fukushima, S. Yuasa, Y. Suzuki, Brownian motion of skyrmion bubbles and its control by voltage applications, Appl. Phys. Lett. 114 (2019), 012402.

[187] A.F. Schäffer, L. Rózsa, J. Berakdar, E.Y. Vedmedenko, R. Wiesendanger, Stochastic dynamics and pattern formation of geometrically confined skyrmions, Commun. Phys. 2 (2019) 1–10.

[188] Y. Jibiki, M. Goto, E. Tamura, J. Cho, S. Miki, R. Ishikawa, H. Nomura, T. Srivastava, W. Lim, S. Auffret, Skyrmion brownian circuit implemented in continuous ferromagnetic thin film, Appl. Phys. Lett. 117 (2020), 082402.

[189] C. Song, N. Kerber, J. Rothörl, Y. Ge, K. Raab, B. Seng, M.A. Brems, F. Dittrich, J. Wang, Q. Liu, Commensurability governing skyrmion diffusion in confined geometries, (2020).

[190] M. Weißenhofer, U. Nowak, Diffusion of skyrmions: the role of topology and anisotropy, New J. Phys. 22 (2020), 103059.

[191] Y. Yao, X. Chen, W. Kang, Y. Zhang, W. Zhao, Thermal Brownian motion of skyrmion for true random number generation, IEEE Trans. Electron Devices 67 (2020) 2553–2558.

[192] L. Zhao, Z. Wang, X. Zhang, X. Liang, J. Xia, K. Wu, H.-A. Zhou, Y. Dong, G. Yu, K. L. Wang, Topology-dependent Brownian gyromotion of a single skyrmion, Phys. Rev. Lett. 125 (2020), 027206.

[193] M. Goto, H. Nomura, Y. Suzuki, Stochastic skyrmion dynamics under alternating magnetic fields, J. Magn. Magn. Mater. 536 (2021), 167974.

[194] N. Kerber, M. Weißenhofer, K. Raab, K. Litzius, J. Zázvorka, U. Nowak, M. Kläui, Anisotropic skyrmion diffusion controlled by magnetic-field-induced symmetry breaking, Phys. Rev. Appl. 15 (2021), 044029.

[195] R. Ishikawa, M. Goto, H. Nomura, Y. Suzuki, Implementation of skyrmion cellular automaton using Brownian motion and magnetic dipole interaction, Appl. Phys. Lett. 119 (2021), 072402.

[196] W.F. Brown Jr, Thermal fluctuations of a single-domain particle, Phys. Rev. 130 (1963) 1677.

[197] J.-V. Kim, F. Garcia-Sanchez, J. Sampaio, C. Moreau-Luchaire, V. Cros, A. Fert, Breathing modes of confined skyrmions in ultrathin magnetic dots, Phys. Rev. B 90 (2014), 064410.

[198] J. Kim, J. Yang, Y.-J. Cho, B. Kim, S.-K. Kim, Coupled breathing modes in one-dimensional Skyrmion lattices, J. Appl. Phys. 123 (2018), 053903.

[199] Y. Zhou, E. Iacocca, A.A. Awad, R.K. Dumas, F. Zhang, H.B. Braun, J. Åkerman, Dynamically stabilized magnetic skyrmions, Nat. Commun. 6 (2015) 8193.

[200] S.-Z. Lin, Dynamics and inertia of a skyrmion in chiral magnets and interfaces: A linear response approach based on magnon excitations, Phys. Rev. B 96 (2017), 014407.

[201] I. Makhfudz, B. Krüger, O. Tchernyshyov, Inertia and chiral edge modes of a skyrmion magnetic bubble, Phys. Rev. Lett. 109 (2012), 217201.

[202] C. Schütte, J. Iwasaki, A. Rosch, N. Nagaosa, Inertia, diffusion, and dynamics of a driven skyrmion, Phys. Rev. B 90 (2014), 174434.

[203] T. Shiino, K.-J. Kim, K.-S. Lee, B.-G. Park, Inertia-driven resonant excitation of a magnetic skyrmion, Sci. Rep. 7 (2017) 1–7.

[204] F. Büttner, C. Moutafis, M. Schneider, B. Krüger, C. Günther, J. Geilhufe, C.v.K. Schmising, J. Mohanty, B. Pfau, S. Schaffert, Dynamics and inertia of skyrmionic spin structures, Nat. Phys., 11 (2015) 225-228.

[205] D. Pinna, G. Bourianoff, K. Everschor-Sitte, Reservoir computing with random skyrmion textures, Phys. Rev. Appl. 14 (2020), 054020.

[206] S. Zhang, X. Zhang, J. Zhang, A. Ganguly, J. Xia, Y. Wen, Q. Zhang, G. Yu, Z. Hou, W. Wang, Direct imaging of an inhomogeneous electric current distribution using the trajectory of magnetic half-skyrmions, Sci. Adv., 6 (2020) eaay1876.

[207] S. Yang, K.W. Moon, C. Kim, D.H. Kim, J. Shin, J. Hong, S.K. Kim, C. Hwang, Control of the Half-Skyrmion Hall Effect and Its Application to Adder-Subtractor, Adv. Quantum Technol. 4 (2021) 2000060.

[208] X. Zhang, Y. Zhou, M. Ezawa, G. Zhao, W. Zhao, Magnetic skyrmion transistor: skyrmion motion in a voltage-gated nanotrack, Sci. Rep. 5 (2015) 1–8.

[209] X. Zhao, R. Ren, G. Xie, Y. Liu, Single antiferromagnetic skyrmion transistor based on strain manipulation, Appl. Phys. Lett. 112 (2018), 252402.

[210] B. Choi, M. Aryal, M. Choi, Y.-K. Hong, Spin–orbit torque driven nano-oscillators based on synthetic Néel-like skyrmion in magnetic tunnel junction, AIP Adv. 12 (2022), 055013.

[211] G. Finocchio, M. Ricci, R. Tomasello, A. Giordano, M. Lanuzza, V. Puliafito, P. Burrascano, B. Azzerboni, M. Carpentieri, Skyrmion based microwave detectors and harvesting, Appl. Phys, Lett. 107 (2015), 262401.

[212] F. Garcia-Sanchez, J. Sampaio, N. Reyren, V. Cros, J. Kim, A skyrmion-based spin-torque nano-oscillator, New J. Phys. 18 (2016), 075011.

[213] J. Guo, J.X. Zhang, P.W. Pong, Y. Wu, H. Chen, W. Zhao, Y. Zhou, A ferromagnetic skyrmion-based nano-oscillator with modified profile of Dzyaloshinskii-Moriya interaction, J. Magn. Magn. Mater. 496 (2020) 165912.

[214] K.Y. Guslienko, Magnetic Skyrmion Spin-Torque Nano-Oscillators, Phys. Status Solidi-Rapid Res. Lett 14 (2020) 2000032.

[215] C. Jin, Y. Ma, C. Song, H. Xia, J. Wang, C. Zhang, Z. Zeng, J. Wang, Q. Liu, High-frequency spin transfer nano-oscillator based on the motion of skyrmions in an annular groove, New J. Phys. 22 (2020), 033001.

[216] C. Jin, J. Wang, W. Wang, C. Song, J. Wang, H. Xia, Q. Liu, Array of synchronized nano-oscillators based on repulsion between domain wall and skyrmion, Phys. Rev. Appl. 9 (2018), 044007.

[217] X. Shi, H. Zhang, Y. Liao, L. Jin, T. Wen, X. Tang, Z. Zhong, Skyrmions based spin-torque nano-oscillator, IEEE Magn. Lett. 8 (2017) 1–5.

[218] S. Zhang, J. Wang, Q. Zheng, Q. Zhu, X. Liu, S. Chen, C. Jin, Q. Liu, C. Jia, D. Xue, Current-induced magnetic skyrmions oscillator, New J. Phys. 17 (2015), 023061.

[219] M.A. Azam, D. Bhattacharya, D. Querlioz, J. Atulasimha, Resonate and fire neuron with fixed magnetic skyrmions, J. Appl. Phys. 124 (2018), 152122.

[220] N. Bindal, C.A.C. Ian, W.S. Lew, B.K. Kaushik, Antiferromagnetic skyrmion repulsion based artificial neuron device, Nanotechnology 32 (2021), 215204.

[221] M.-C. Chen, A. Sengupta, K. Roy, Magnetic skyrmion as a spintronic deep learning spiking neuron processor, IEEE Trans. Magn. 54 (2018) 1–7.

[222] X. Chen, W. Kang, D. Zhu, X. Zhang, N. Lei, Y. Zhang, Y. Zhou, W. Zhao, A compact skyrmionic leaky–integrate–fire spiking neuron device, Nanoscale 10 (2018) 6139–6146.

[223] D. Das, Y. Cen, J. Wang, X. Fong, Bilayer-Skyrmion based design of Neuron and Synapse for Spiking Neural Network, arXiv preprint arXiv:2203.02171, (2022).

[224] Z. He, D. Fan, Developing all-skyrmion spiking neural network, arXiv preprint arXiv:1705.02995, (2017).

[225] Z. He, D. Fan, A tunable magnetic skyrmion neuron cluster for energy efficient artificial neural network, in: Design, Automation & Test in Europe Conference & Exhibition (DATE), 2017, IEEE, 2017, pp. 350-355.

[226] S. Li, W. Kang, Y. Huang, X. Zhang, Y. Zhou, W. Zhao, Magnetic skyrmion-based artificial neuron device, Nanotechnology 28 (2017) 31LT01.

[227] M.-M. Zhu, S.-T. Cui, X.-F. Xu, S.-B. Shi, D.-Q. Nian, J. Luo, Y. Qiu, H. Yang, G.-L. Yu, H.-M. Zhou, Voltage-controllable magnetic skyrmion dynamics for spiking neuron device applications, Chin. Phys. B 31 (2022), 018503.

[228] X. Liang, X. Zhang, J. Xia, M. Ezawa, Y. Zhao, G. Zhao, Y. Zhou, A spiking neuron constructed by the skyrmion-based spin torque nano-oscillator, Appl. Phys, Lett. 116 (2020), 122402.

[229] T. Bhattacharya, S. Li, Y. Huang, W. Kang, W. Zhao, M. Suri, Low-power (1t1n) skyrmionic synapses for spiking neuromorphic systems, IEEE Access 7 (2019) 5034–5044.

[230] C. Chen, T. Lin, J. Niu, Y. Sun, L. Yang, W. Kang, N. Lei, Surface acoustic wave controlled skyrmion-based synapse devices, Nanotechnology 33 (2021), 115205.

[231] R. Chen, C. Li, Y. Li, J.J. Miles, G. Indiveri, S. Furber, V.F. Pavlidis, C. Moutafis, Nanoscale room-temperature multilayer skyrmionic synapse for deep spiking neural Networks, Phys. Rev. Appl. 14 (2020), 014096.

[232] Y. Huang, W. Kang, X. Zhang, Y. Zhou, W. Zhao, Magnetic skyrmion-based synaptic devices, Nanotechnology 28 (2017) 08LT02.

[233] S.-G. Je, P. Vallobra, T. Srivastava, J.-C. Rojas-Sánchez, T.H. Pham, M. Hehn, G. Malinowski, C. Baraduc, S. Auffret, G. Gaudin, Creation of magnetic skyrmion bubble lattices by ultrafast laser in ultrathin films, Nano Lett. 18 (2018) 7362–7371.

[234] K.M. Song, J.-S. Jeong, B. Pan, X. Zhang, J. Xia, S. Cha, T.-E. Park, K. Kim, S. Finizio, J. Raabe, Skyrmion-based artificial synapses for neuromorphic computing, Nat. Electron. 3 (2020) 148–155.

[235] G. Bourianoff, D. Pinna, M. Sitte, K. Everschor-Sitte, Potential implementation of reservoir computing models based on magnetic skyrmions, AIP Adv. 8 (2018), 055602.

[236] X. Chen, F.A. Araujo, M. Riou, J. Torrejon, D. Ravelosona, W. Kang, W. Zhao, J. Grollier, D. Querlioz, Forecasting the outcome of spintronic experiments with Neural Ordinary Differential Equations, Nat. Commun. 13 (2022) 1016.

[237] W. Jiang, L. Chen, K. Zhou, L. Li, Q. Fu, Y. Du, R. Liu, Physical reservoir computing using magnetic skyrmion memristor and spin torque nano-oscillator, Appl. Phys, Lett. 115 (2019), 192403.

[238] M.-K. Lee, M. Mochizuki, Reservoir Computing with Spin Waves in Skyrmion Crystal, arXiv preprint arXiv:2203.02160, (2022).

[239] J. Love, J. Mulkers, G. Bourianoff, J. Leliaert, K. Everschor-Sitte, Task Agnostic Metrics for Reservoir Computing, arXiv preprint arXiv:2108.01512, (2021).

[240] D. Prychynenko, M. Sitte, K. Litzius, B. Krüger, G. Bourianoff, M. Kläui, J. Sinova, K. Everschor-Sitte, Magnetic skyrmion as a nonlinear resistive element: a potential building block for reservoir computing, Phys. Rev. Appl. 9 (2018), 014034.

[241] M.M. Rajib, W.A. Misba, M. Chowdhury, F. Fahim, M.S. Alam, J. Atulasimha, Skyrmion based energy efficient straintronic physical reservoir computing, arXiv preprint arXiv:2112.13527, (2021).

[242] T. Yokouchi, S. Sugimoto, B. Rana, S. Seki, N. Ogawa, Y. Shiomi, S. Kasai, Y. Otani, Pattern recognition with neuromorphic computing using magnetic-field induced dynamics of skyrmions, arXiv preprint arXiv:2204.13260, (2022).

[243] H. Zhang, D. Zhu, W. Kang, Y. Zhang, W. Zhao, Stochastic computing implemented by skyrmionic logic devices, Phys. Rev. Appl. 13 (2020), 054049.

[244] I. Medlej, A. Hamadeh, F.E.H. Hassan, Skyrmion based random bit generator, Phys. B: Condens. Matter 579 (2020), 411900.

[245] S.I. Kiselev, J. Sankey, I. Krivorotov, N. Emley, R. Schoelkopf, R. Buhrman, D. Ralph, Microwave oscillations of a nanomagnet driven by a spin-polarized current, Nature 425 (2003) 380–383.

[246] V. Pribiag, I. Krivorotov, G. Fuchs, P. Braganca, O. Ozatay, J. Sankey, D. Ralph, R. Buhrman, Magnetic vortex oscillator driven by dc spin-polarized current, Nat. Phys. 3 (2007) 498–503.

[247] K.Y. Guslienko, Magnetic vortex state stability, reversal and dynamics in restricted geometries, J. Nanosci. Nanotechnol. 8 (2008) 2745–2760.

[248] Q. Mistral, M. van Kampen, G. Hrkac, J.-V. Kim, T. Devolder, P. Crozat, C. Chappert, L. Lagae, T. Schrefl, Current-driven vortex oscillations in metallic nanocontacts, Phys. Rev. Lett. 100 (2008), 257201.

[249] A. Khvalkovskiy, J. Grollier, A. Dussaux, K.A. Zvezdin, V. Cros, Vortex oscillations induced by spin-polarized current in a magnetic nanopillar: Analytical versus micromagnetic calculations, Phys. Rev. B 80 (2009), 140401.

[250] A. Ruotolo, V. Cros, B. Georges, A. Dussaux, J. Grollier, C. Deranlot, R. Guillemet, K. Bouzehouane, S. Fusil, A. Fert, Phase-locking of magnetic vortices mediated by antivortices, Nat. Nanotechnol. 4 (2009) 528–532.

[251] G.R. Aranda, J.M. Gonzalez, J.J. del Val, K.Y. Guslienko, Limits for the vortex state spin torque oscillator in magnetic nanopillars: Micromagnetic simulations for a thin free layer, J. Appl. Phys. 108 (2010), 123914.

[252] E. Grimaldi, A. Dussaux, P. Bortolotti, J. Grollier, G. Pillet, A. Fukushima, H. Kubota, K. Yakushiji, S. Yuasa, V. Cros, Response to noise of a vortex based spin transfer nano-oscillator, Phys. Rev. B 89 (2014), 104404.

[253] P. Livi, G. Indiveri, A current-mode conductance-based silicon neuron for address-event neuromorphic systems, in: 2009 IEEE international symposium on circuits and systems, IEEE, 2009, pp. 2898-2901.

[254] P. Merolla, J. Arthur, F. Akopyan, N. Imam, R. Manohar, D.S. Modha, A digital neurosynaptic core using embedded crossbar memory with 45pJ per spike in 45nm, in: 2011 IEEE custom integrated circuits conference (CICC), IEEE, 2011, pp. 1-4.

[255] X. Wu, V. Saxena, K. Zhu, S. Balagopal, A CMOS spiking neuron for brain-inspired neural networks with resistive synapses and in situ learning, IEEE Trans. Circuits Syst. II (62) (2015) 1088–1092.

[256] S.H. Jo, T. Chang, I. Ebong, B.B. Bhadviya, P. Mazumder, W. Lu, Nanoscale memristor device as synapse in neuromorphic systems, Nano Lett. 10 (2010) 1297–1301.

[257] T. Tuma, A. Pantazi, M. Le Gallo, A. Sebastian, E. Eleftheriou, Stochastic phase-change neurons, Nat. Nanotechnol. 11 (2016) 693–699.

[258] D. Kuzum, R.G. Jeyasingh, B. Lee, H.-S.-P. Wong, Nanoelectronic programmable synapses based on phase change materials for brain-inspired computing, Nano Lett. 12 (2012) 2179–2186.

[259] A. Sengupta, A. Banerjee, K. Roy, Hybrid spintronic-CMOS spiking neural network with on-chip learning: Devices, circuits, and systems, Phys. Rev. Appl. 6 (2016), 064003.

[260] A. Sengupta, Z. Al Azim, X. Fong, K. Roy, Spin-orbit torque induced spike-timing dependent plasticity, Appl. Phys, Lett., 106 (2015) 093704.

[261] R.M. Borisyuk, G.N. Borisyuk, Information coding on the basis of synchronization of neuronal activity, BioSystems 40 (1997) 3–10.

[262] A. Jaiswal, A. Agrawal, P. Panda, K. Roy, Voltage-driven domain-wall motion based neuro-synaptic devices for dynamic on-line learning, arXiv preprint arXiv: 1705.06942, (2017).

[263] P. Stoliar, J. Tranchant, B. Corraze, E. Janod, M.P. Besland, F. Tesler, M. Rozenberg, L. Cario, A leaky-integrate-and-fire neuron analog realized with a Mott insulator, Adv. Funct. Mater. 27 (2017) 1604740.

[264] G.W. Burr, R.M. Shelby, A. Sebastian, S. Kim, S. Kim, S. Sidler, K. Virwani, M. Ishii, P. Narayanan, A. Fumarola, Neuromorphic computing using non-volatile memory, Adv. Phys.: X 2 (2017) 89–124.

[265] S. Song, K.D. Miller, L.F. Abbott, Competitive Hebbian learning through spike-timing-dependent synaptic plasticity, Nat. Neurosci. 3 (2000) 919–926.

[266] Z. Yu, M. Shen, Z. Zeng, S. Liang, Y. Liu, M. Chen, Z. Zhang, Z. Lu, L. You, X. Yang, Voltage-controlled skyrmion-based nanodevices for neuromorphic computing using a synthetic antiferromagnet, Nanoscale Adv. 2 (2020) 1309–1317.

[267] S. Luo, N. Xu, Z. Guo, Y. Zhang, J. Hong, L. You, Voltage-controlled skyrmion memristor for energy-efficient synapse applications, IEEE Electron Device Lett. 40 (2019) 635–638.

[268] K.Y. Camsari, B.M. Sutton, S. Datta, P-bits for probabilistic spin logic, Appl. Phys. Rev. 6 (2019), 011305.

[269] A. Mizrahi, T. Hirtzlin, A. Fukushima, H. Kubota, S. Yuasa, J. Grollier, D. Querlioz, Neural-like computing with populations of superparamagnetic basis functions, Nat. Commun. 9 (2018) 1533.

[270] M. Yamaoka, C. Yoshimura, M. Hayashi, T. Okuyama, H. Aoki, H. Mizuno, A 20k-spin Ising chip to solve combinatorial optimization problems with CMOS annealing, IEEE J. Solid-State Circuits 51 (2015) 303–309.

[271] K. Kim, M.-S. Chang, S. Korenblit, R. Islam, E.E. Edwards, J.K. Freericks, G.-D. Lin, L.-M. Duan, C. Monroe, Quantum simulation of frustrated Ising spins with trapped ions, Nature 465 (2010) 590–593.

[272] I. Mahboob, H. Okamoto, H. Yamaguchi, An electromechanical ising hamiltonian, Sci. Adv. 2 (2016), e1600236.

[273] A. Marandi, Z. Wang, K. Takata, R.L. Byer, Y. Yamamoto, Network of time-multiplexed optical parametric oscillators as a coherent Ising machine, Nat. Photonics 8 (2014) 937–942.

[274] P.L. McMahon, A. Marandi, Y. Haribara, R. Hamerly, C. Langrock, S. Tamate, T. Inagaki, H. Takesue, S. Utsunomiya, K. Aihara, A fully programmable 100-spin coherent Ising machine with all-to-all connections, Science 354 (2016) 614–617.

[275] T. Inagaki, Y. Haribara, K. Igarashi, T. Sonobe, S. Tamate, T. Honjo, A. Marandi, P.L. McMahon, T. Umeki, K. Enbutsu, A coherent Ising machine for 2000-node optimization problems, Science 354 (2016) 603–606.

[276] B. Sutton, K.Y. Camsari, B. Behin-Aein, S. Datta, Intrinsic optimization using stochastic nanomagnets, Sci. Rep. 7 (2017) 1–9.

[277] B. Behin-Aein, V. Diep, S. Datta, A building block for hardware belief networks, Sci. Rep. 6 (2016) 1–10.

[278] U.B. Arnalds, J. Chico, H. Stopfel, V. Kapaklis, O. Bärenbold, M.A. Verschuuren, U. Wolff, V. Neu, A. Bergman, B. Hjörvarsson, A new look on the two-dimensional Ising model: thermal artificial spins, New J. Phys. 18 (2016), 023008.

[279] G. Tanaka, T. Yamane, J.B. Héroux, R. Nakane, N. Kanazawa, S. Takeda, H. Numata, D. Nakano, A. Hirose, Recent advances in physical reservoir computing: A review, Neural Netw. 115 (2019) 100–123.

[280] H. Soh, Y. Demiris, Iterative temporal learning and prediction with the sparse online echo state gaussian process, in: The 2012 international joint conference on neural networks (IJCNN), IEEE, 2012, pp. 1-8.

[281] Y. Paquot, F. Duport, A. Smerieri, J. Dambre, B. Schrauwen, M. Haelterman, S. Massar, Optoelectronic reservoir computing, Sci. Rep. 2 (2012) 1–6.

[282] D. Verstraeten, B. Schrauwen, D. Stroobandt, J. Van Campenhout, Isolated word recognition with the liquid state machine: a case study, Inf. Process. Lett. 95 (2005) 521–528.

[283] A. Jalalvand, G. Van Wallendael, R. Van de Walle, Real-time reservoir computing network-based systems for detection tasks on visual contents, in: 2015 7th International Conference on Computational Intelligence, Communication Systems and Networks, IEEE, 2015, pp. 146-151.

[284] H. Jaeger, The "echo state" approach to analysing and training recurrent neural networks-with an erratum note, Bonn, Germany: German National Research Center for Information Technology GMD Technical Report 148 (2001) 13.

[285] H. Jaeger, Adaptive nonlinear system identification with echo state networks, Adv. Neural Inf. Process. Syst. 15 (2002).

[286] H. Hauser, A.J. Ijspeert, R.M. Füchslin, R. Pfeifer, W. Maass, The role of feedback in morphological computation with compliant bodies, Biol. Cybern. 106 (2012) 595–613.

[287] H. Jaeger, Tutorial on training recurrent neural networks, covering BPPT, RTRL, EKF and the" echo state network" approach, GMD-Forschungszentrum Informationstechnik Bonn, 2002.

[288] H. Jaeger, H. Haas, Harnessing nonlinearity: Predicting chaotic systems and saving energy in wireless communication, Science (2004).

[289] N. Bertschinger, T. Natschläger, Real-time computation at the edge of chaos in recurrent neural networks, Neural Comput. 16 (2004) 1413–1436.

[290] H. Jaeger, Short term memory in echo state networks. gmd-report 152, in: GMD-German National Research Institute for Computer Science (2002), Citeseer, 2002.

[291] M.C. Soriano, S. Ortín, L. Keuninckx, L. Appeltant, J. Danckaert, L. Pesquera, G. Van der Sande, Delay-based reservoir computing: noise effects in a combined analog and digital implementation, IEEE Trans. Neural Netw. Learn. Syst. 26 (2014) 388–393.

[292] L. Appeltant, M.C. Soriano, G. Van der Sande, J. Danckaert, S. Massar, J. Dambre, B. Schrauwen, C.R. Mirasso, I. Fischer, Information processing using a single dynamical node as complex system, Nat. Commun. 2 (2011) 468.

[293] G. Van der Sande, D. Brunner, M.C. Soriano, Advances in photonic reservoir computing, Nanophotonics 6 (2017) 561–576.

[294] T. Taniguchi, S. Tsunegi, S. Miwa, K. Fujii, H. Kubota, K. Nakajima, Reservoir Computing Based on Spintronics Technology, in, Reservoir Computing, Springer (2021) 331–360.

[295] H. Hauser, Physical Reservoir Computing in Robotics, in: Reservoir Computing, Springer, 2021, pp. 169-190.

[296] Y. Kharkov, O. Sushkov, M. Mostovoy, Bound states of skyrmions and merons near the Lifshitz point, Phys. Rev. Lett. 119 (2017), 207201.

[297] B. Göbel, A. Mook, J. Henk, I. Mertig, O.A. Tretiakov, Magnetic bimerons as skyrmion analogues in in-plane magnets, Phys. Rev. B 99 (2019), 060407.

[298] N. Gao, S.-G. Je, M.-Y. Im, J.W. Choi, M. Yang, Q.-C. Li, T. Wang, S. Lee, H.-S. Han, K.-S. Lee, Creation and annihilation of topological meron pairs in in-plane magnetized films, Nat. Commun. 10 (2019) 5603.

[299] B. Göbel, I. Mertig, O.A. Tretiakov, Beyond skyrmions: Review and perspectives of alternative magnetic quasiparticles, Phys. Rep. 895 (2021) 1–28.

[300] E.Y. Vedmedenko, P. Riego, J.A. Arregi, A. Berger, Interlayer dzyaloshinskii-moriya interactions, Phys. Rev. Lett. 122 (2019), 257202.

[301] A. Fernández-Pacheco, E. Vedmedenko, F. Ummelen, R. Mansell, D. Petit, R.P. Cowburn, Symmetry-breaking interlayer Dzyaloshinskii-Moriya interactions in synthetic antiferromagnets, Nat. Mater. 18 (2019) 679–684.

[302] K. Wang, L. Qian, S.-C. Ying, G. Xiao, Spin-orbit torque switching of chiral magnetization across a synthetic antiferromagnet, Commun. Phys. 4 (2021) 1–7.

[303] D.-S. Han, K. Lee, J.-P. Hanke, Y. Mokrousov, K.-W. Kim, W. Yoo, Y.L. Van Hees, T.-W. Kim, R. Lavrijsen, C.-Y. You, Long-range chiral exchange interaction in synthetic antiferromagnets, Nat. Mater. 18 (2019) 703–708.

[304] S. Li, W. Kang, X. Zhang, T. Nie, Y. Zhou, K.L. Wang, W. Zhao, Magnetic skyrmions for unconventional computing, Materials Horizons 8 (2021) 854–868.